# SYMMETRY AND AUTOMATED BRANCH FOLLOWING FOR A SEMILINEAR ELLIPTIC PDE ON A FRACTAL REGION

JOHN M. NEUBERGER, NÁNDOR SIEBEN, AND JAMES W. SWIFT

Abstract. We apply the Gradient-Newton-Galerkin-Algorithm (GNGA) of Neuberger & Swift to find solutions to a semilinear elliptic Dirichlet problem on the region whose boundary is the Koch snowflake. In a recent paper, we described an accurate and efficient method for generating a basis of eigenfunctions of the Laplacian on this region. In that work, we used the symmetry of the snowflake region to analyze and post-process the basis, rendering it suitable for input to the GNGA. The GNGA uses Newton's method on the eigenfunction expansion coefficients to find solutions to the semilinear problem. This article introduces the *bifurcation digraph*, an extension of the lattice of isotropy subgroups. For our example, the bifurcation digraph shows the 23 possible symmetry types of solutions to the PDE and the 59 generic symmetry-breaking bifurcations among these symmetry types. Our numerical code uses continuation methods, and follows branches created at symmetry-breaking bifurcations, so the human user does not need to supply initial guesses for Newton's method. Starting from the known trivial solution, the code automatically finds at least one solution with each of the symmetry types that we predict can exist. Such computationally intensive investigations necessitated the writing of automated branch following code, whereby symmetry information was used to reduce the number of computations per GNGA execution and to make intelligent branch following decisions at bifurcation points.

## 1. Introduction.

We seek numerical solutions to the semilinear elliptic boundary value problem

$$\begin{aligned} \Delta u + f_\lambda(u) &= 0 \text{ in } \Omega \\ u &= 0 \text{ on } \partial\Omega, \end{aligned} \tag{1}$$

where $\Delta$ is the Laplacian operator, $\Omega \subset \mathbb{R}^2$ is the region whose boundary $\partial\Omega$ is the Koch snowflake, $u : \Omega \to \mathbb{R}$ is the unknown function, and $f_\lambda : \mathbb{R} \to \mathbb{R}$ is a one-parameter family of odd functions. For convenience, we refer to $\Omega$ as the *Koch snowflake region*. This article is one of the first to consider a nonlinear PDE on a region with fractal boundary. In this paper, we choose the nonlinearity to be

$$f_\lambda(u) = \lambda u + u^3, \tag{2}$$

and treat $\lambda \in \mathbb{R}$ as the bifurcation parameter. When the parameter is fixed, we will sometimes use $f$ in place of $f_\lambda$. Using this convention, note that $\lambda = f'(0)$.

This paper exploits the hexagonal symmetry of the Koch snowflake region, and the fact that $f$ is odd. Our nonlinear code would work with any region with hexagonal symmetry and any odd 'superlinear' function $f$ (see [4]), and with minor modification for other classes of nonlinearities as well. We chose to work with odd $f$ primarily because of the rich symmetry structure. The explicit shape of $\Omega$ represents a considerable technological challenge for the computation of the eigenfunctions [16, 27], which are required as input to the nonlinear code.

It is well known that the eigenvalues of the Laplacian under this boundary condition satisfy

$$0 < \lambda_1 < \lambda_2 \leq \lambda_3 \leq \cdots \to \infty, \tag{3}$$

2000 *Mathematics Subject Classification.* 20C35, 35P10, 65N25.

*Key words and phrases.* Snowflake, Symmetry, Bifurcation, Semilinear Elliptic PDE, GNGA.

Partially supported by NSF Grant DMS-0074326.

October 7, 2010.

and that the corresponding eigenfunctions $\{\psi_j\}_{j\in\mathbb{N}}$ can be chosen to be an orthogonal basis for the Sobolev space $H = H_0^1(\Omega) = W_0^{1,2}(\Omega)$, and an orthonormal basis for the larger Hilbert space $L^2 = L^2(\Omega)$. The inner products are

$$\langle u, v\rangle_H = \int_\Omega \nabla u \cdot \nabla v \, dx \quad \text{and} \quad \langle u, v\rangle_2 = \int_\Omega u \, v \, dx,$$

respectively (see [1, 9, 15, 17]). Theorem 8.37 and subsequent remarks in [9] imply that the eigenfunctions are in $C^\infty(\Omega)$. In [17], properties of the gradients of eigenfunctions near boundary points are explored in light of the lack of regularity of $\partial\Omega$.

Using the Gradient-Newton-Galerkin-Algorithm (GNGA, see [26]) we seek approximate solutions $u = \sum_{j=1}^M a_j\psi_j$ to (1) by applying Newton's method to the eigenfunction expansion coefficients of the gradient $\nabla J(u)$ of a nonlinear functional $J$ whose critical points are the desired solutions. The definition of $J$, the required variational equations, a description of the GNGA, and a brief history of the problem are the subject of Section 2.

The GNGA requires as input a basis spanning a sufficiently large but finite dimensional subspace $B_M = \text{span}\{\psi_1, \ldots, \psi_M\}$, corresponding to the first $M$ eigenvalues $\{\lambda_j\}_{j=1}^M$. As described in [27], a grid $G_N$ of $N$ carefully placed points is used to approximate the eigenfunctions. These are the same grid points used for the numerical integrations required by Newton's method. Section 3 briefly describes the process we use for generating the eigenfunctions.

Section 4 concerns the effects of symmetry on automated branch following. The symmetry theory for linear operators found in [27] is summarized and then the extensions required for nonlinear operators are described. Symmetry-breaking bifurcations are analyzed in a way that allows an automated system to follow the branches created at the bifurcations. As we develop the theory, we present specific examples applying the general theory to equation (1) on the snowflake region. In particular, we find that there are 23 different symmetry types of solutions to (1), and 59 generic symmetry-breaking bifurcations. The symmetry types and bifurcations among them are summarized in a *bifurcation digraph*, which generalizes the well-known lattice of isotropy subgroups (see [10]). As far as we know, the bifurcation digraph is a new way to organize the information about the symmetry-breaking bifurcations.

Section 5 describes how understanding the symmetry allows remarkable increases in the efficiency of the GNGA. Section 6 describes the automated branch following. We use repeated executions of the GNGA or a slightly modified algorithm (parameter-modified GNGA) to follow solution branches of (1, 2). The GNGA uses Newton's method, which is known to work well if it has a good initial approximation. The main shortcoming of Newton's method is that is works poorly without a good initial approximation. We avoid this problem by starting with the trivial solution ($u = 0$). The symmetry-breaking bifurcations of the trivial solution are found by the algorithm and the primary branches are started. The program follows the branches by continuation methods, and then follows the new branches created at symmetry-breaking bifurcations. To follow an existing branch, we vary $\lambda$ slightly between executions. To start new solution branches created at bifurcation points, we treat $\lambda$ as a variable and fix one of the null eigenfunctions of the Hessian evaluated at the bifurcation point. The symmetry analysis tells which null eigenfunction to use. In this way solutions with all 23 symmetry types are found automatically, starting from $u = 0$, without having to guess any approximations for Newton's method.

In our experiments, many bifurcation diagrams were generated by applying the techniques mentioned above. A selection of these diagrams are provided in Section 7, along with contour plots of solutions to (1) corresponding to each of the 23 symmetry types predicted to exist. We include evidence of the convergence of our algorithm as the number of modes $M$ and grid points $N$ increase.

Many extensions to our work are possible, including enforcing different boundary conditions on the same region, solving similar semilinear equations on other fractal regions, and applying the methodology to partial difference equations (PdE) on graphs [25]. Section 8 discusses some of these possible extensions. In particular, we are in the process of re-writing the suite of programs.

We plan to be able to solve larger problems using a parallel environment. We will be able to solve problems with larger symmetry groups by automating the extensive group theoretic calculations. This concluding section also has a discussion of the convergence of the GNGA.

## 2. GNGA.

We now present the variational machinery for studying (1) and follow with a brief description of the general GNGA. Section 6 contains more details of the implementation of the algorithm for our specific problem. Let $F_\lambda(u) = \int_0^u f_\lambda(s)\,ds$ for all $u \in \mathbb{R}$ define the primitive of $f_\lambda$. We then define the action functional $J : \mathbb{R} \times H \to \mathbb{R}$ by

$$J(\lambda, u) = \int_\Omega \left\{ \tfrac{1}{2}|\nabla u|^2 - F_\lambda(u) \right\} dx. \tag{4}$$

We will sometimes use $J : H \to \mathbb{R}$ to denote $J(\lambda, \cdot)$. The class of nonlinearities $f$ found in [4, 5, 25, 28] imply that $J$ is well defined and of class $C^2$ on $H$. The choice (2) we make in this paper belongs to that class. Critical points of $J$ are by definition weak solutions of (1) (see for example [4, 28, 9]), and clearly classical solutions are critical points. The usual "bootstrap" argument of repeatedly applying Theorem 8.10 of [9] can be used in our case. Specifically, $H_0^k$ is embedded in $L^q$ for all $q \geq 2$ when the space diminsion $n$ is 2, regardless of the regularity of $\partial\Omega$ (due to the zero Dirichlet boundary condition, see [1]). Hence $u \in H^k$ implies $f(u) \in H^k$ as well. As a result, if $u$ is a critical point then $u \in C^\infty(\Omega) \cap C(\bar{\Omega})$, hence a classical solution. If one considered boundary conditions, space dimensions, and nonlinear terms other than the choices made in this paper, it could happen that critical points would be weak not classicial solutions. Regardless, our approximations lie in $B_M \subset C^\infty$. Here, the existence proofs for positive, negative, and sign-changing exactly once solutions from [4, 28] immediately give at least 3 nontrivial (classical) solutions for our specific superlinear boundary value problem; appealing to symmetry implies the existence of even more solutions (see for example [25]).

The choice of $H$ for the domain is crucial to the analysis of the PDE (see [4, 24], and references therein), as well as for understanding the theoretical basis of effective steepest descent algorithms (see [7, 22, 23], for example). We will work in the coefficient space $\mathbb{R}^M \cong B_M$. The *coefficient vector of* $u \in B_M$ is the vector $a \in \mathbb{R}^M$ satisfying $u = \sum_{j=1}^M a_j \psi_j$. Using the corresponding eigenvalues (3) and integrating by parts, the quantities of interest are

$$g_j = J'(u)(\psi_j) = \int_\Omega \{\nabla u \cdot \nabla \psi_j - f(u)\,\psi_j\} = a_j \lambda_j - \int_\Omega f(u)\,\psi_j, \quad \text{and} \tag{5}$$

$$h_{jk} = J''(u)(\psi_j, \psi_k) = \int_\Omega \{\nabla \psi_j \cdot \nabla \psi_k - f'(u)\,\psi_j\,\psi_k\} = \lambda_j \delta_{jk} - \int_\Omega f'(u)\,\psi_j\,\psi_k, \tag{6}$$

where $\delta_{jk}$ is the Kronecker delta function. Note that there is no need for numerical differentiation when forming gradient and Hessian coefficient vectors and matrices in implementing Algorithm 2.1; this information is encoded in the eigenfunctions.

The vector $g \in \mathbb{R}^M$ and the $M \times M$ matrix $h$ represent suitable projections of the $L^2$ gradient and Hessian of $J$, restricted to the subspace $B_M$, where all such quantities are defined. For example, for $u = \sum_{j=1}^M a_j \psi_j$, $v = \sum_{j=1}^M b_j \psi_j$, and $w = \sum_{j=1}^M c_j \psi_j$, we have:

$$P_{B_M} \nabla_2 J(u) = \sum_{j=1}^M g_j \psi_j, \;\; J'(u)(v) = g \cdot b, \text{ and } J''(u)(v, w) = hb \cdot c = b \cdot hc.$$

We can identify $g$ with the approximation $P_{B_M} \nabla_2 J(u)$ of $\nabla_2 J(u) = \Delta u + f(u)$, which is defined for $u \in B_M$. The solution $\chi$ to the $M$-dimensional linear system $h\chi = g$ is then identified with the (suitably projected) search direction $(D_2^2 J(u))^{-1} \nabla_2 J(u)$, which is not only defined for $u \in B_M$, but is there equal to $(D_H^2 J(u))^{-1} \nabla_H J(u)$. We use the least squares solution of $h\chi = g$. In practice, the algorithm works even near bifurcation points where the Hessian is not invertible.

The heart of our code is Newton's method in the space of eigenfunction coefficients:

*Algorithm* 2.1. (GNGA)

(1) Choose initial coefficients $a = \{a_j\}_{j=1}^M$, and set $u = \sum a_j \psi_j$.
(2) Loop
  (a) Calculate the gradient vector $g = \{J'(u)(\psi_j)\}_{j=1}^M$ from equation (5).
  (b) Calculate the Hessian matrix $h = \{J''(u)(\psi_j, \psi_k)\}_{j,\,k=1}^M$ from equation (6).
  (c) Exit loop if $||g||$ is sufficiently small.
  (d) Solve $h\chi = g$ for the Newton search direction $\chi \in \mathbb{R}^M$.
  (e) Replace $a \leftarrow a - \chi$ and update $u = \sum a_j \psi_j$.
(3) Calculate $\mathrm{sig}(h)$ and $J$ for the approximate solution.

If Newton's method converges then we expect that $u$ approximates a solution to the PDE (1), provided $M$ is sufficiently large and the eigenfunctions and numerical integrations are sufficiently accurate. See Section 8.

Our estimate for the Morse index (MI) of the critical point of $J$ is the signature of $h$, denoted $\mathrm{sig}(h)$, which is defined as the number of negative eigenvalues of $h$. This measures the number of linearly independent directions away from $u$ in which $J$ decreases quadratically.

The basic Algorithm 2.1 is modified to take advantage of the symmetry of our problem. The $M$ integrations required in step (a) and the $M(M+1)/2$ integrations in step (b) are reduced to fewer integrations if the initial guess has nontrivial symmetry.

We often use a "parameter-modified" version of the GNGA (pmGNGA). In this modification, $\lambda$ is treated as an unknown variable and one of the $M$ coefficients $a_k$ is fixed. Along a given branch, symmetry generally forces many coefficients to be zero. When a bifurcation point is located by observing a change in MI, we can predict the symmetry of the bifurcating branches using the symmetry of the null eigenfunctions of the Hessian. By forcing a small nonzero component in the direction of a null eigenfunction (orthogonal to the old branch's smaller invariant subspace), we can assure that the pmGNGA will not converge to a solution lying on the old branch. Another benefit of the pmGNGA is that it can handle a curve bifurcating to the right as well as one bifurcating to the left. In our system, the branches that bifurcate to the right have saddle node bifurcations where they turn around and go to the left. The pmGNGA can follow such branches while the normal GNGA cannot.

The implementation of pmGNGA is not difficult. The $M$ equations are still

$$g_i = J'(u)(\psi_i) = 0,$$

but the $M$ unknowns are

$$\tilde{a} = (a_1, \ldots, a_{k-1}, \lambda, a_{k+1}, \ldots, a_M),$$

and the value of one coefficient, $a_k$, is fixed. Consequently, we replace the Hessian matrix $h$ with a new matrix $\tilde{h}$ where the $k$-th column is set to $\partial g_i/\partial\lambda = -a_i$:

$$\tilde{h}_{ij} = \begin{cases} h_{ij} & \text{if } j \neq k \\ -a_i & \text{if } j = k \end{cases}.$$

The search direction $\tilde{\chi}$ is the solution to the system $\tilde{h}\tilde{\chi} = g$. The pmGNGA step is

$$\tilde{a} \leftarrow \tilde{a} - \tilde{\chi},$$

and then $u$ and $\lambda$ are updated. After Newton's method converges, the $k$-th column of the original $h_{ij}$ is calculated and the MI of the solution, $\mathrm{sig}(h)$, is computed.

We conclude this section with a very brief history of the analytical and numerical aspects of the research into (1) given our type of nonlinearity $f$. Our introduction to this general subject was [4], where a sign-changing existence result was proven. This theorem is extended in [5]; we indicate briefly in Section 7 where this so-called CCN solution can be found on our bifurcation diagrams. The article [7] was our first success in using symmetry to find higher MI solutions. The

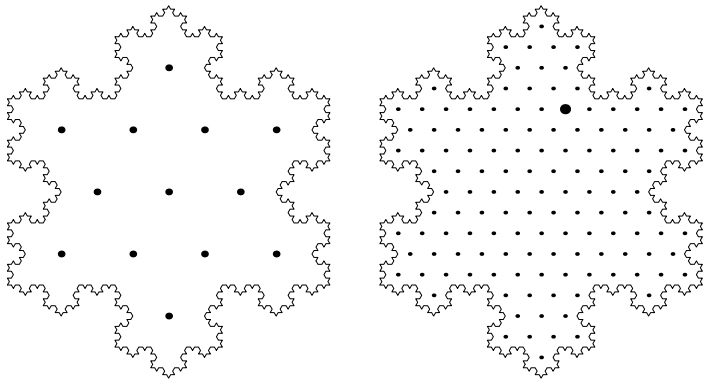

FIGURE 1. The Koch snowflake region $\Omega$ with the grids $G_{13}$ and $G_{133}$ at levels $\ell = 2$ and 3, respectively. A generic grid point (which is not on any line of reflection symmetry) is indicated in the larger grid.

GNGA was developed in [26], wherein a much more detailed description of the variational structure and numerical implementation can be found. The first implementation of the GNGA for regions where the eigenfunctions are not known in closed form is in [12], where the region is a Bunimovich stadium. The article [24] provides a historical overview of the authors' experimental results using variants of the Mountain Pass Algorithm (MPA, MMPA, HLA) and the GNGA, as well as recent analytical results and a list of open problems; the references found therein are extensive.

## 3. The Basis of Eigenfunctions.

In [27], we describe theoretical and computational results that lead to the generation of a basis of eigenfunctions solving

$$\Delta u + \lambda u = 0 \text{ in } \Omega, \quad u = 0 \text{ on } \partial\Omega. \tag{7}$$

That paper details the grid technique and symmetry analysis that accompanied the effort; we briefly summarize those results in this section.

The Koch snowflake is a well-known fractal, with Hausdorff dimension $\log_3 4$. Following Lapidus, Neuberger, Renka, and Griffith [16], we take our snowflake to be inscribed in a circle of radius $\frac{\sqrt{3}}{3}$ centered about the origin. We use a triangular grid $G_N$ of $N$ points to approximate the snowflake region. Then, we identify $u : G_N \to \mathbb{R}$ with $u \in \mathbb{R}^N$, that is,

$$u(x_i) = u_i \tag{8}$$

at grid points $x_i \in G_N$. Our paper [27] differs from [16] in that we use a different placement of the grid points and a different method of enforcing the boundary condition, resulting in more accurate eigenvalue estimates with fewer points. Figure 1 depicts the levels 2 and 3 grids in the family of grids used in [27] to compute eigenfunctions; we used the first $M$ eigenfunctions computed at levels 4, 5, and 6 in our nonlinear experiments. The number of grid points at level $\ell$ is $N = (9^\ell - 4^\ell)/5$, and the spacing between grid points is $h = 2/3^\ell$. We computed the eigenvalues and eigenfunctions for (7) using ARPACK and this approximation to the Laplacian with zero-Dirichlet boundary conditions:

$$-\Delta u(x) \approx \frac{2}{3h^2}\left((12 - \text{number of neighbors})\, u(x) - \sum\{\text{neighboring values of } u\}\right). \tag{9}$$

The ARPACK is based upon an algorithmic variant of the Arnoldi process called the Implicitly Restarted Arnoldi Method (see [19]) and is ideally suited for finding the eigen-pairs of the large sparse matrices associated with the discretization of the Laplacian.

## 4. Symmetry: The Lattice of Isotropy Subgroups and The Bifurcation Digraph.

This section describes equivariant bifurcation theory as it applies to the branching of solutions to equation (1), see [6, 10, 11, 18]. We are able to describe the expected symmetry types of solutions to (1), as traditionally arranged in a lattice of isotropy subgroups. We introduce the *bifurcation digraph*, a refinement of the lattice, which shows every possible generic bifurcation from one symmetry type to another as a directed edge which is labeled with information about the bifurcation. The bifurcation digraph is of interest in its own right and summarizes the essential information required by our automated branch following code. In this project, GAP (Groups, Algorithms, and Programming, see [8]) was used solely to verify the symmetry analysis we did by hand. In our continuing projects GAP is a useful tool since it can perform the tedious calculations and write the information in a format that can be read by the branch following code. Matthews [21] has used GAP to do similar calculations. We apply this methodology to the snowflake domain being considered in this paper. The analysis shows that solutions fall into 23 symmetry types, and that there are 59 types of generic symmetry breaking bifurcations.

**Group Actions and the Lattice of Isotropy Subgroups.** Let $\Gamma$ be a finite group and $V$ be a real vector space. A *representation* of $\Gamma$ is a homomorphism $\alpha : \Gamma \to GL(V)$. Where convenient, we identify $GL(V)$ with the set of invertible matrices with real coefficients. Every representation $\alpha$ corresponds to a unique *group action* of $\Gamma$ on $V$ by the rule $\gamma \cdot v := \alpha(\gamma)(v)$ for all $\gamma \in \Gamma$ and $v \in V$. We will usually use the action rather than the representation. The *group orbit* of $v$ is $\Gamma \cdot v = \{\gamma \cdot v \mid \gamma \in \Gamma\}$.

*Example* 4.1. Let

$$\mathbb{D}_6 := \langle \rho, \sigma \mid \rho^6 = \sigma^2 = 1,\, \rho\,\sigma = \sigma\rho^5 \rangle$$

be the dihedral group with 12 elements. It is convenient to define $\tau = \rho^3\sigma$. It follows that $\sigma\tau = \tau\sigma = \rho^3$. The group $\mathbb{D}_6$ is the symmetry of a regular hexagon, and of the Koch Snowflake region $\Omega$. The standard $\mathbb{D}_6$ action on the plane is given by

$$\begin{aligned} \rho \cdot (x,y) &= \left(\tfrac{1}{2}x + \tfrac{\sqrt{3}}{2}y, -\tfrac{\sqrt{3}}{2}x + \tfrac{1}{2}y\right) \\ \sigma \cdot (x,y) &= (-x, y) \\ \tau \cdot (x,y) &= (x, -y). \end{aligned} \tag{10}$$

In this action, $\rho$ is a rotation by 60°, $\sigma$ is a reflection across the $y$-axis, and $\tau$ is a reflection across the $x$-axis. These group actions are depicted in Figure 13, near the end of the paper.

We will denote subgroups of $\mathbb{D}_6$ by listing the generators. While any given subgroup of $\mathbb{D}_6$ can be defined using only $\rho$ and $\sigma$, we find it geometrically descriptive to use $\tau$ in certain cases. For example, we prefer $\langle \rho^2, \tau \rangle$ to the equivalent $\langle \rho^2, \rho\sigma \rangle$. In order to make relationships among subgroups intuitive, we often include $\tau$ when its membership is implied by the other generators (see for example Figure 2).

The standard $\mathbb{D}_6$ group action (10) is not the only action we consider. For a function $u \in L^2(\Omega)$ and group element $\gamma \in \mathbb{D}_6$, we define $(\gamma \cdot u)(x) = u(\gamma^{-1} \cdot x)$. In this paper, a vector $u$ defined by $u_i = u(x_i)$, for a given grid $G_N = \{x_i\}_{i=1}^N$, is a discrete approximation of a function on $\Omega$. The $\mathbb{D}_6$ group action on $u \in \mathbb{R}^N$ is a permutation of the components: $(\gamma \cdot u)_i = u(\gamma^{-1} \cdot x_i)$. Given a function $u \in L^2(\Omega)$ or $\mathbb{R}^N$, the group orbit $\mathbb{D}_6 \cdot u$ consists of functions obtained from $u$ by a reflection or rotation.

*Example* 4.2. The group $\mathbb{D}_6 \times \mathbb{Z}_2$, where $\mathbb{Z}_2 = \{1, -1\}$, acts on $L^2(\Omega)$ in a natural way. For all $(\gamma, z) \in \mathbb{D}_6 \times \mathbb{Z}_2$, define

$$(\gamma, z) \cdot u = z(\gamma \cdot u).$$

We will denote $(\gamma, 1) \in \mathbb{D}_6 \times \mathbb{Z}_2$ by $\gamma$ and $(\gamma, -1) \in \mathbb{D}_6 \times \mathbb{Z}_2$ by $-\gamma$. With this natural notation $(-\gamma) \cdot u = -(\gamma \cdot u)$, which we call simply $-\gamma \cdot u$.

Let us recall some facts about group actions, following [6, 10, 11]. The *isotropy subgroup* or *stabilizer of* $v \in V$ *in* $\Gamma$ is

$$\mathrm{Stab}(v, \Gamma) := \{\gamma \in \Gamma \mid \gamma \cdot v = v\}.$$

The isotropy subgroup measures the symmetry of $v$, and is sometimes called the little group of $v$, or $\Gamma_v$. If the group $\Gamma$ is understood, we may simply write $\mathrm{Stab}(v)$ in place of $\mathrm{Stab}(v, \Gamma)$. The *stabilizer of a subset* $W \subseteq V$ *in* $\Gamma$ is $\mathrm{Stab}(W, \Gamma) := \{\gamma \in \Gamma \mid \gamma \cdot W = W\}$. This must be distinguished from the *point stabilizer of a subset*

$$\mathrm{pStab}(W, \Gamma) := \{\gamma \in \Gamma \mid \gamma \cdot v = v \text{ for all } v \in W\} = \bigcap \{\mathrm{Stab}(v, \Gamma) \mid v \in W\}.$$

Another commonly used notation is $\Gamma_W$ for the stabilizer and $\Gamma_{(W)}$ for the point stabilizer. Note that $\mathrm{pStab}(W, \Gamma)$ is always normal in $\mathrm{Stab}(W, \Gamma)$, and the *effective symmetry group acting on* $W$ is $\mathrm{Stab}(W, \Gamma)/\mathrm{pStab}(W, \Gamma)$, which acts faithfully on $W$.

If $\Sigma$ is a subgroup of $\Gamma$ then the *fixed point subspace of* $\Sigma$ *in* $V$ is

$$\mathrm{Fix}(\Sigma, V) := \{v \in V \mid \ \gamma \cdot v = v \text{ for all } \gamma \in \Sigma\}.$$

Another notation for the fixed point subspace is $V_\Sigma$. We write $\mathrm{Fix}(\Sigma)$ when $V$ is understood.

An *isotropy subgroup* of the $\Gamma$ action on $V$ is the stabilizer of some point $v \in V$. For some group actions, not every subgroup of $\Gamma$ is an isotropy subgroup.

*Example* 4.3. Consider the $\mathbb{D}_6$ action on the plane $\mathbb{R}^2$ described in equation (10. It is well-known that $\langle \rho \rangle$ is not an isotropy subgroup of this action.

Now consider the $\mathbb{D}_6$ action on the function space $L^2(\Omega)$. We give a standard argument that every subgroup of $\mathbb{D}_6$ is an isotropy subgroup. Start with a function $u^*$ that is zero everywhere except for a small region, and suppose that the region is distinct from each of its nontrivial images under the $\mathbb{D}_6$ action. Then for any subgroup $\Sigma \leq \mathbb{D}_6$, the *average of the function* $u^*$ *over* $\Sigma$, defined as

$$P_\Sigma(u^*) = \frac{1}{|\Sigma|} \sum_{\gamma \in \Sigma} \gamma \cdot u^* \tag{11}$$

has isotropy subgroup $\Sigma$. Therefore every subgroup of the $\mathbb{D}_6$ action on $L^2(\Omega)$ is an isotropy subgroup. The average over the group is an example of a Haar operator, and $P_\Sigma : V \to \mathrm{Fix}(\Sigma, V)$ is an orthogonal projection operator [36].

Similarly, every subgroup of $\mathbb{D}_6$ is an isotropy subgroup of the $\mathbb{D}_6$ action on $\mathbb{R}^N$, the space of functions on the grid $G_N$, provided $\ell \geq 3$. This follows from averaging the function that is 1 at a generic lattice point, and 0 elsewhere. Recall that a *generic point* is one whose isotropy subgroup is trivial. Figure 1 shows that the level two grid $G_{13}$ does not have a generic point, while the level three grid $G_{133}$ does. Thus, the space of functions on $G_{133}$ has the same isotropy subgroups as $L^2(\Omega)$, but a much smaller space has this same property. Start with any generic point $x_1 \in \Omega$. Then $\mathbb{D}_6$ acts on the space of functions on the 12 points $\mathbb{D}_6 \cdot x_1$. This $\mathbb{D}_6$ action on $\mathbb{R}^{12}$ has the same structure of isotropy subgroups as the $\mathbb{D}_6$ action on $L^2(\Omega)$, and is the $\mathbb{D}_6$ action used in our GAP calculations. The corresponding 12-dimensional representation is the well-known *regular representation* of $\mathbb{D}_6$ (see [29, 31, 34]).

The symmetry of functions is described by two related concepts. A function $q : V \to \mathbb{R}$ is $\Gamma$-*invariant* if $q(\gamma \cdot v) = q(v)$ for all $\gamma \in \Gamma$ and all $v \in V$. Similarly, an operator $T : V \to V$ is $\Gamma$-*equivariant* if $T(\gamma \cdot v) = \gamma \cdot T(v)$ for all $\gamma \in \Gamma$ and all $v \in V$.

*Example* 4.4. The energy functional $J$ defined in equation (4) is $\mathbb{D}_6 \times \mathbb{Z}_2$-invariant. The nonlinear PDE (1) can be written as $(\Delta + f)(u) = 0$, where $\Delta + f$ is a $\mathbb{D}_6 \times \mathbb{Z}_2$-equivariant operator. (There are subtleties concerning the domain and range of $\Delta$. See [6, 7] for a careful treatment of the function spaces.) In particular, $\Delta + f$ is $\mathbb{D}_6$-equivariant because the snowflake region $\Omega$ has $\mathbb{D}_6$ symmetry, and $(\Delta + f)(-u) = -(\Delta + f)(u)$, since $f$ is odd. As a consequence, if $u$ is a solution to (1), then so is every element in its group orbit $(\mathbb{D}_6 \times \mathbb{Z}_2) \cdot u$.

The isotropy subgroups and fixed point subspaces are important because of the following simple yet powerful results. See [6, 10, 11].

**Proposition 4.5.** *Suppose* $\Gamma$ *acts linearly on* $V$*,* $T : V \to V$ *is* $\Gamma$*-equivariant and* $\Sigma$ *is an isotropy subgroup of* $\Gamma$*.*

(a) *If* $v \in \mathrm{Fix}(\Sigma)$ *then* $T(v) \in \mathrm{Fix}(\Sigma)$*. Thus,* $T|_{\mathrm{Fix}(\Sigma)} : \mathrm{Fix}(\Sigma) \to \mathrm{Fix}(\Sigma)$ *is defined.*
(b) $\mathrm{Stab}(\mathrm{Fix}(\Sigma)) = N_\Gamma(\Sigma)$*, the normalizer of* $\Sigma$ *in* $\Gamma$*, and* $\mathrm{pStab}(\mathrm{Fix}(\Sigma)) = \Sigma$*.*
(c) $T|_{\mathrm{Fix}(\Sigma)}$ *is* $N_\Gamma(\Sigma)$*-equivariant.*
(d) $T|_{\mathrm{Fix}(\Sigma)}$ *is* $N_\Gamma(\Sigma)/\Sigma$*-equivariant, and* $N_\Gamma(\Sigma)/\Sigma$ *acts faithfully on* $\mathrm{Fix}(\Sigma)$*.*

If $\Sigma$ is a subgroup of $\Gamma$, the normalizer of $\Sigma$ in $\Gamma$ is defined to be $N_\Gamma(\Sigma) := \{\gamma \in \Gamma \mid \gamma\Sigma = \Sigma\gamma\}$, which is the largest subgroup of $\Gamma$ for which $\Sigma$ is a normal subgroup. The presence of the normalizer in Proposition 4.5(b) is interesting, since the normalizer is a property of the abstract groups, and is independent of the group action.

*Example* 4.6. As a consequence of Proposition 4.5, we can solve the PDE (1), written as $(\Delta+f)(u) = 0$, by restricting $u$ to functions in $\mathrm{Fix}(\Sigma, L^2(\Omega))$. This leads to a simpler problem since the function space $\mathrm{Fix}(\Sigma, L^2(\Omega))$ is simpler than $L^2(\Omega)$. An example of this is in Costa, Ding, and Neuberger [7]. The techniques of that paper, applied to our problem, would find sign-changing solutions with Morse index 2 within the space $\mathrm{Fix}(\mathbb{D}_6, L^2(\Omega))$. This space consists of all functions which are unchanged under all of the rotations and reflections of the snowflake region.

Proposition (4.5) also applies to the GNGA, since the Newton's method iteration mapping is $\mathbb{D}_6 \times \mathbb{Z}_2$-equivariant. If the initial guess is in a particular fixed point subspace, all the iterates will be in that fixed point subspace. This fact can be used to speed numerical calculations, as described in Section 5.

Two subgroups $\Sigma_1, \Sigma_2$ of $\Gamma$ are conjugate ($\Sigma_1 \sim \Sigma_2$) if $\Sigma_1 = \gamma\Sigma_2\gamma^{-1}$ for some $\gamma \in \Gamma$. The *symmetry type* of $v \in V$ for the $\Gamma$ action is the conjugacy class of $\mathrm{Stab}(v, \Gamma)$. Note that $\mathrm{Stab}(\gamma \cdot v) = \gamma\,\mathrm{Stab}(v)\gamma^{-1}$. Thus, every element of a group orbit $\Gamma \cdot v$ has the same symmetry type.

Let $\mathcal{S} = \{S_i\}$ denote the set of all symmetry types of a $\Gamma$ action on $V$. The set $\mathcal{S}$ has a natural partial order, with $S_i \le S_j$ if there exits $\Sigma_i \in S_i$ and $\Sigma_j \in S_j$ such that $\Sigma_i \le \Sigma_j$. The partially ordered set $(\mathcal{S}, \le)$ is called the *lattice of isotropy subgroups* of the $\Gamma$ action on $V$ [10]. The *diagram* of the lattice of isotropy subgroups is a directed graph with vertices $S_i$ and arrows $S_i \leftarrow S_j$ if, and only if, $S_i \lneq S_j$ and there is no symmetry type between $S_i$ and $S_j$.

*Example* 4.7. The symmetry type of a solution $u$ to our PDE (1) for the $\mathbb{D}_6 \times \mathbb{Z}_2$ action is the conjugacy class of $\mathrm{Stab}(u, \mathbb{D}_6 \times \mathbb{Z}_2)$; we refer to this as the symmetry type of $u$, without reference to $\mathbb{D}_6 \times \mathbb{Z}_2$. The discussion of $\mathbb{D}_6$ acting on $L^2(\Omega)$ in Example 4.3 can easily be extended to $\mathbb{D}_6 \times \mathbb{Z}_2$ acting on $L^2(\Omega)$. Note that if $-1 \in \Sigma \le \mathbb{D}_6 \times \mathbb{Z}_2$, then the average of any function over $\Sigma$ is $u = 0$. Therefore the only isotropy subgroup of $\mathbb{D}_6 \times \mathbb{Z}_2$ which contains $-1$ is $\mathbb{D}_6 \times \mathbb{Z}_2$ itself. On the other hand, the argument in Example 4.3 shows that any subgroup of $\mathbb{D}_6 \times \mathbb{Z}_2$ which does not contain $-1$ is an isotropy subgroup. Therefore, $\Sigma \le \mathbb{D}_6 \times \mathbb{Z}_2$ is an isotropy subgroup of this group action if and only if $\Sigma = \mathbb{D}_6 \times \mathbb{Z}_2$ or $-1 \notin \Sigma$.

This result allowed us to compute the isotropy subgroups by hand. We verified our calculations using GAP. There are exactly 23 conjugacy classes of isotropy subgroups for the $\mathbb{D}_6 \times \mathbb{Z}_2$ action on $L^2(\Omega)$, shown in condensed form in Figure 2. Thus, a solution to the PDE (1) has one of 23 different symmetry types.

**Irreducible Representations and the Isotypic Decomposition.** In order to understand the symmetry-breaking bifurcations we need to first understand irreducible representations and the isotypic decomposition of a group action. The information about the irreducible representations is summarized in character tables [29, 31, 32, 34]. For our purposes, irreducible representations over the field $\mathbb{R}$ are required, see [6, 10, 11]. The *irreducible representations of* $\Gamma$ are homomorphisms from $\Gamma$ to the space of $d_j \times d_j$ real matrices: $\gamma \mapsto \alpha^{(j)}(\gamma)$, such that no proper subspace of $\mathbb{R}^{d_j}$ is

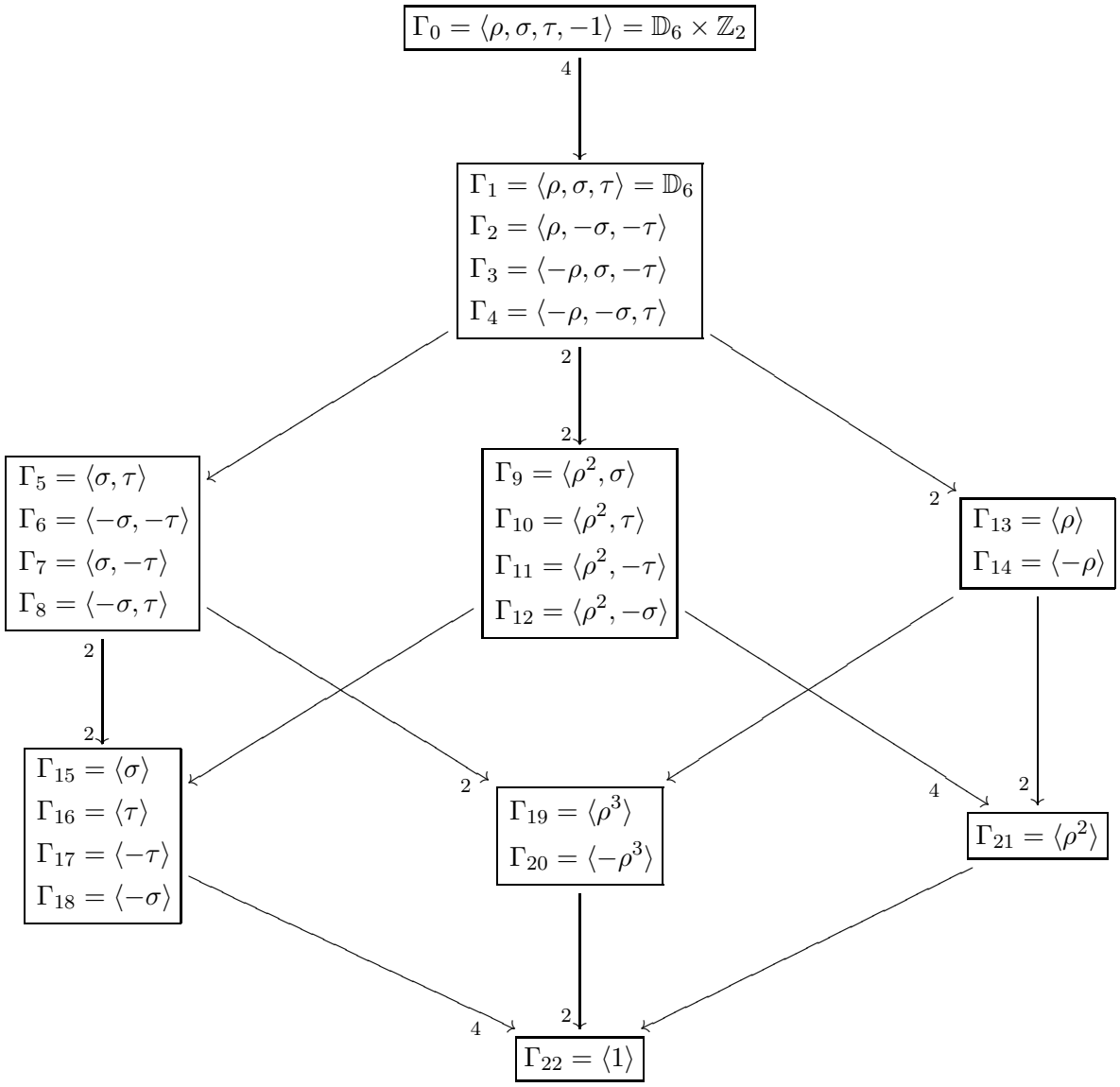


FIGURE 2. The condensed diagram of the isotropy lattice (see [10]) for the $\mathbb{D}_6 \times \mathbb{Z}_2$ action on $L^2(\Omega)$. The vertices of this diagram are the symmetry types (equivalence classes of isotropy subgroups). We follow the convention [6, 10, 11] that one element $\Gamma_i$ of each symmetry type $S_i = [\Gamma_i]$ is listed. The representatives $\Gamma_i$ have the property that $\Gamma_i \leq \Gamma_j$ iff $S_i \leq S_j$. Contour plots of solutions to PDE (1) with each of the 23 symmetry types are given in Figures 13 and 14. The diagram of the isotropy lattice is condensed as in [32]. The small numbers on the edges tell the number of connections emanating from each symmetry type in a box. A missing small number means 1. For example, the two arrows representing $[\Gamma_{21}] \leq [\Gamma_{13}]$ and $[\Gamma_{21}] \leq [\Gamma_{14}]$ in the full diagram are collapsed to a single arrow in the condensed diagram. For $\Gamma_0$ through $\Gamma_4$, the $\tau$ generator is redundant since $\tau = \rho^3\sigma$, but its presence makes the subgroups manifest. For example, $\Gamma_2 = \langle \rho, -\sigma, -\tau \rangle = \langle \rho, -\sigma \rangle$, but the three generators make it clear that $\langle -\sigma, -\tau \rangle \leq \langle \rho, -\sigma, -\tau \rangle$.

invariant under $\alpha^{(j)}(\gamma)$ for all $\gamma \in \Gamma$. The *dimension of the irreducible representation* $\alpha^{(j)}$ is $d_j$. We call $W \subseteq V$ a $\Gamma$-*invariant subspace of* $V$ if $\Gamma \cdot W \subseteq W$. An *irreducible subspace of* $V$ is an invariant subspace with no proper invariant subspaces. Every irreducible subspace of the $\Gamma$ action on $V$ corresponds to a unique (up to similarity) irreducible representation of $\Gamma$. The dimension of the irreducible subspace is the same as the dimension of the corresponding irreducible representation.

For each irreducible representation $\alpha^{(j)}$ of $\Gamma$, the *isotypic component* of $V$ for the $\Gamma$ action, denoted by $V_\Gamma^{(j)}$, is defined to be the direct sum of all of the irreducible subspaces corresponding to the fixed $\alpha^{(j)}$ [6, 10, 11, 27]. The *isotypic decomposition* of $V$ is then

$$V = \bigoplus_j V_\Gamma^{(j)}. \tag{12}$$

Some of the isotypic components might be the single point at the origin. These can be left out of the isotypic decomposition. A description of the isotypic components in terms of projection operators is given in [27].

For any group $\Gamma$, we denote the trivial representation by $\alpha^{(1)}$. That is $\alpha^{(1)}(\gamma) = 1$ for all $\gamma \in \Gamma$. Thus, if $\Gamma$ is an isotropy subgroup of a $\Gamma_0$ action on $V$, then

$$V_\Gamma^{(1)} = \mathrm{Fix}(\Gamma, V).$$

*Example* 4.8. Let us consider the $\mathbb{D}_6 = \langle \rho, \sigma, \tau \rangle$ action on $L^2(\Omega)$. We need to consider the six irreducible representations of $\mathbb{D}_6$, which are listed in [27], to find the isotypic decomposition of $L^2(\Omega)$. Since these isotypic components are central to our problem, we drop the $\mathbb{D}_6$ and define $V^{(j)} := V_{\mathbb{D}_6}^{(j)}$, $j = 1, 2, \ldots, 6$ as follows:

$$\begin{aligned}
V^{(1)} &= \{u \in L^2(\Omega) \mid \rho \cdot u = u,\ \sigma \cdot u = u,\ \tau \cdot u = u\} \\
V^{(2)} &= \{u \in L^2(\Omega) \mid \rho \cdot u = u,\ \sigma \cdot u = -u,\ \tau \cdot u = -u\} \\
V^{(3)} &= \{u \in L^2(\Omega) \mid \rho \cdot u = -u,\ \sigma \cdot u = u,\ \tau \cdot u = -u\} \\
V^{(4)} &= \{u \in L^2(\Omega) \mid \rho \cdot u = -u,\ \sigma \cdot u = -u,\ \tau \cdot u = u\} \\
V^{(5)} &= \{u \in L^2(\Omega) \mid \rho^3 \cdot u = u,\ u + \rho^2 \cdot u + \rho^4 \cdot u = 0\} \\
V^{(6)} &= \{u \in L^2(\Omega) \mid \rho^3 \cdot u = -u,\ u + \rho^2 \cdot u + \rho^4 \cdot u = 0\}.
\end{aligned} \tag{13}$$

*Example* 4.9. The isotypic decomposition of $\Gamma_{13} = \langle \rho \rangle \cong \mathbb{Z}_6$ illustrates some features of *real* representation theory. The irreducible representations of $\mathbb{Z}_6$ over $\mathbb{C}$ are all one-dimensional. They are $\alpha^{(j)}(\rho) = (e^{i\pi/3})^{j-1}$ for $j = 1, 2, \ldots, 6$. Over the field $\mathbb{R}$, however, the one-dimensional irreducible representations of $\mathbb{Z}_6$ are given by

$$\alpha^{(1)}(\rho) = 1, \quad \alpha^{(2)}(\rho) = -1, \tag{14}$$

and the two-dimensional irreducible representations of $\mathbb{Z}_6$, up to similarity transformations, are given by

$$\alpha^{(3)}(\rho) = \begin{pmatrix} -\frac{1}{2} & \frac{\sqrt{3}}{2} \\ -\frac{\sqrt{3}}{2} & -\frac{1}{2} \end{pmatrix}, \quad \alpha^{(4)}(\rho) = \begin{pmatrix} \frac{1}{2} & \frac{\sqrt{3}}{2} \\ -\frac{\sqrt{3}}{2} & \frac{1}{2} \end{pmatrix}. \tag{15}$$

Note that $\alpha^{(3)}(\rho)$ is matrix for a rotation by 120° and $\alpha^{(4)}(\rho)$ is a 60° rotation matrix.

An irreducible representation over $\mathbb{R}$ is called *absolutely irreducible* if it is also irreducible over $\mathbb{C}$. For example, all of the irreducible representations of $\mathbb{D}_6$ listed in [27] are absolutely irreducible, as are the one-dimensional irreducible representations of $\mathbb{Z}_6$ in equation (14). On the other hand, the two-dimensional irreducible representations of $\mathbb{Z}_6$ in equation (15) are *not* absolutely irreducible.

The four isotypic components of the $\langle \rho \rangle$ action on $L^2(\Omega)$ are

$$V_{\langle \rho \rangle}^{(1)} = \{u \in L^2(\Omega) \mid \rho \cdot u = u\} = V^{(1)} \oplus V^{(2)}$$

$$V^{(2)}_{\langle\rho\rangle} = \{u \in L^2(\Omega) \mid \rho \cdot u = -u\} = V^{(3)} \oplus V^{(4)}$$
$$V^{(3)}_{\langle\rho\rangle} = V^{(5)}, \text{ and } V^{(4)}_{\langle\rho\rangle} = V^{(6)}.$$

If we had used the complex irreducible representations, some of the corresponding isotypic components would contain complex-valued functions. It is more natural to use real irreducible representations, and consider only real-valued functions. The price we pay is that most of the representation theory found in books, and built into GAP, is done for complex irreducible representations.

The isotypic decomposition for each of the 23 isotropy subgroups, $\Gamma_i$, of $\mathbb{D}_6 \times \mathbb{Z}_2$ can be written as a direct sum of some subset of the eight spaces $V^{(j)}$, for $j = 1, \ldots, 4$, and $V_1^{(j)}$ and $V_2^{(j)}$ for $j = 5, 6$ defined in (13) and [27]. The C++ program can easily check if a function is in any of the isotypic components $V^{(j)}_{\Gamma_i}$ of $B_M$ for each of the $\Gamma_i$, $i = 0, 1, \ldots, 22$, actions.

**Symmetry-Breaking Bifurcations.** The fact that there are 23 *possible* symmetry types of solutions to the PDE (1) begs the question, do solutions with each of these symmetry types exist? Clearly the trivial solution $u = 0$, with symmetry type $S_0$, exits. Our procedure for finding approximate solutions with each of these symmetry types is to start with the trivial solution and recursively follow solution branches created at symmetry-breaking bifurcations.

Let us start by abstracting the PDE defined by (1), which depends on the real parameter $\lambda$. Let $V$ be an inner product space and $J : \mathbb{R} \times V \to \mathbb{R}$ be a family of $\Gamma_0-$invariant functions that depends on a parameter $\lambda$. That is, $J(\lambda, \gamma \cdot u) = J(\lambda, u)$ for all $\gamma \in \Gamma_0$ and $u \in V$. It is understood that $\Gamma_0$ is the *largest* known group for which $J$ is invariant; of course $J$ is also invariant under any subgroup of $\Gamma_0$. We will use $\Gamma$, or $\Gamma_i$, to refer to an isotropy subgroup of the "full" group $\Gamma_0$. Consider the steady-state bifurcation problem $g(\lambda, u) = 0$, where $g(\lambda, u) = \nabla J(\lambda, u)$. Throughout this paper, the gradient $\nabla$ acts on the $u$ component. The solutions to $g(\lambda, u) = 0$ are critical points of $J$, so we use the terms "solution" and "critical point" interchangeably. Note that $g : \mathbb{R} \times V \to V$ is a family of $\Gamma_0-$equivariant gradient operators on $V$. That is, $g(\lambda, \gamma \cdot u) = \gamma \cdot g(\lambda, u)$. For our PDE, $\Gamma_0 = \mathbb{D}_6 \times \mathbb{Z}_2$. In the numerical implementation, $V = \mathbb{R}^M \cong B_M$ and $g$ is defined in (5).

We define a *branch of solutions* to be a connected component of $\{(\lambda, u) \in \mathbb{R} \times L^2(\Omega) \mid g(\lambda, u) = 0,\ \mathrm{Stab}(u) = \Gamma\}$, where $\Gamma$ is called the isotropy subgroup, or symmetry, of the branch. A branch of solutions $B_1$ has a *symmetry-breaking bifurcation* at the *bifurcation point* $(\lambda^*, u^*) \in B_1$ if a branch of solutions, $B_2$, with a different symmetry, has $(\lambda^*, u^*)$ as a limit point but $(\lambda^*, u^*) \notin B_2$. We say that branch $B_2$ is *created* at this bifurcation, and often refer to $B_1$ as the *mother branch* and $B_2$ as the *daughter branch*. The symmetry of the daughter branch is always a proper subgroup of the symmetry of the mother branch. That is, the daughter has less symmetry than the mother.

The main tool for finding bifurcation points is the Hessian of the energy functional, $h$. If $(\lambda^*, u^*)$ is a bifurcation point, then $h(\lambda^*, u^*)$ is not invertible, since otherwise the implicit function theorem would guarantee the existence of a unique local solution branch. The *Morse index* (MI) of a critical point $(\lambda, u)$ is defined to be the number of negative eigenvalues of $h(\lambda, u) = D^2 J(\lambda, u)$, provided no eigenvalue is 0. The Hessian is symmetric, so all of its eigenvalues are real. The MI on a branch of solutions typically changes at a bifurcation point.

*Example* 4.10. The trivial solution to (1, 2) is $u = 0$, and the *trivial branch* is $\{(\lambda, 0) \mid \lambda \in \mathbb{R}\}$. Since $h(\lambda, 0)(v) = \Delta v + \lambda v$, the bifurcation points of the trivial branch are $(\lambda_i, 0)$, where $\lambda_i, i \in \mathbb{N}$, are the eigenvalues (3). If $\lambda_i < \lambda < \lambda_{i+1}$, then the MI of the trivial solution $(\lambda, 0)$ is $i$. The $i$-th *primary branch* is created at the bifurcation point $(\lambda_i, 0)$ on the trivial branch. In cases with double eigenvalues there are two branches created at the same point in our problem. For example, the second and third primary branches are created at $\lambda_2 = \lambda_3$. Near $(\lambda_i, 0)$, the solutions on the $i$-th primary branch are approximately some constant times the $i$-th eigenfunction of the Laplacian, $\psi_i$.

We define a *degenerate critical point*, or a *degenerate solution*, to be a point $(\lambda^*, u^*)$ which satisfies $g(\lambda^*, u^*) = 0$ and $\det h(\lambda^*, u^*) = 0$. Thus, every bifurcation point is a degenerate critical point. Some degenerate critical points are not bifurcation points. For example, when a branch

folds over and is not monotonic in $\lambda$, the *fold point* is degenerate, but is not a bifurcation point as we have defined it. (Note that we avoid the term "saddle-node bifurcation" since there is really no bifurcation.)

Let us develop some notation to talk about bifurcations. Suppose that $(\lambda^*, u^*)$ is an isolated degenerate critical point of a $\Gamma_0$-equivariant system $g(\lambda, u) = 0$. Let $\Gamma = \mathrm{Stab}(u^*, \Gamma_0)$, and define $L := h(\lambda^*, u^*)$. Note that $\Gamma$, not $\Gamma_0$, is important as far as the bifurcation of $(\lambda^*, u^*)$ is concerned. Let $E$ be the null space of the $\Gamma$-equivariant operator $L$. We call $E$ the *center eigenspace*. Let $\Gamma'$ be the point stabilizer of $E$. The definitions are repeated here for reference:

$$\Gamma := \mathrm{Stab}(u^*, \Gamma_0),\ L := h(\lambda^*, u^*),\ E := N(L),\ \Gamma' := \mathrm{pStab}(E, \Gamma). \tag{16}$$

If $e \in E$, then $L(e) = 0$ by definition. For any $\gamma \in \Gamma$, $\gamma \cdot e \in E$ since the $\Gamma$-equivariance of $L$ implies that $L(\gamma \cdot e) = \gamma \cdot L(e) = 0$. Hence,

$$\mathrm{Stab}(E, \Gamma) = \Gamma.$$

Note that $\mathrm{Stab}(E, \Gamma)/\,\mathrm{pStab}(E, \Gamma) = \Gamma/\Gamma'$ acts faithfully on $E$. In the usual case where $(\lambda^*, u^*)$ is a bifurcation point, not just a degenerate critical point, we say that $\Gamma/\Gamma'$ is the *symmetry group of the bifurcation*, or that $(\lambda^*, u^*)$ undergoes a *bifurcation with* $\Gamma/\Gamma'$ *symmetry*.

In the notation of (16), $L$ sends each of the isotypic components $V_\Gamma^{(j)}$ to itself [27, 31, 34]. Barring "accidental degeneracy," the center eigenspace $E$ is a $\Gamma$-irreducible subspace. Thus, $E$ is typically a subspace of exactly one isotypic component $V_\Gamma^{(j)}$, and $\dim(E)$ is the dimension $d_j$ of the corresponding corresponding irreducible representation, $\alpha^{(j)}$. Furthermore, the point stabilizer of $E$ is the kernel of $\alpha^{(j)}$ and can be computed without knowing $E$. In summary, at a generic bifurcation point there is some irreducible representation $\alpha^{(j)}$ of $\Gamma$ such that:

$$E \text{ is } \Gamma\text{-irreducible}, \quad E \subseteq V_\Gamma^{(j)}, \quad \dim(E) = \Delta MI = d_j, \quad \Gamma' = \{\gamma \in \Gamma \mid \alpha^{(j)}(\gamma) = I\}.$$

Accidental degeneracy is discussed in [27, 31, 34]. We did not encounter any accidental degeneracy in our numerical investigation of (1, 2), so we will not discuss it further here.

We finally have the background to describe the bifurcations which occur in equivariant systems. The goal is to predict what solutions will be created at each of the symmetry breaking bifurcations, and know what vectors in $E$ to use to start these branches using the pmGNGA. While such a prediction is impossible for some complicated groups, we can determine how to follow all of the bifurcating branches in the system (1, 2). We follow the treatment and notation of [10, 11]. At a symmetry-breaking bifurcation we can translate $(\lambda^*, u^*)$ to the origin, and we could, in principle, do an equivariant Liapunov-Schmidt reduction or center manifold reduction to obtain reduced bifurcation equations $\tilde{g} : \mathbb{R} \times E \to E$ where $\tilde{g}(0, 0) = 0$, $D\tilde{g}(0, 0) = 0$, and $\tilde{g}$ is $\Gamma := \mathrm{Stab}(u^*)$-equivariant. It is important to realize that we do not actually need to perform the Liapunov-Schmidt reduction.

The most powerful tool for understanding symmetry breaking bifurcations is the Equivariant Branching Lemma. Recall that absolutely irreducible representations were defined in Example 4.9. See [6, 10, 11] for a thorough discussion of the Equivariant Branching Lemma, including further references.

**Theorem 4.11. Equivariant Branching Lemma (EBL)** *Suppose* $\Gamma$ *acts absolutely irreducibly on the space* $E$*, and let* $\tilde{g} : \mathbb{R} \times E \to E$ *be* $\Gamma$*-equivariant. Assume that* $\Gamma$ *acts nontrivially, so* $\tilde{g}(\lambda, 0) = 0$*. Since* $\Gamma$ *acts absolutely irreducibly,* $D\tilde{g}(\lambda, 0) = c(\lambda) I_d$ *for some function* $c : \mathbb{R} \to \mathbb{R}$*, where* $I_d$ *is the identity matrix of size* $d = \dim(E)$*. Assume that* $c(0) = 0$ *and* $c'(0) \neq 0$*. Let* $\Sigma$ *be an isotropy subgroup of the* $\Gamma$ *action on* $E$ *with* $\dim \mathrm{Fix}(\Sigma, E) = 1$*. Then there are at least two solution branches of* $\tilde{g}(\lambda, u) = 0$ *with isotropy subgroup* $\Sigma$ *created at* $(0, 0)$*.*

The EBL, combined with Liapunov-Schmidt theory, implies that there are at least two solution branches of the full problem $g(\lambda, u) = 0$ with isotropy subgroup $\Sigma$ created at the bifurcation point $(\lambda^*, u^*)$. We call these newly created branches *EBL branches* since their existence can be predicted by the EBL. Other branches created at a bifurcation are called *non-EBL branches*.

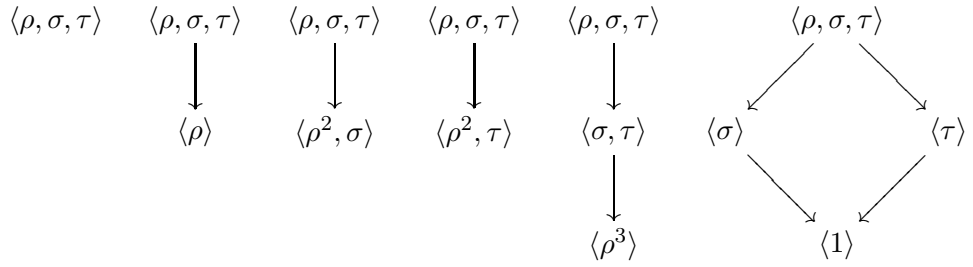


FIGURE 3. Diagrams of the six isotropy lattices for the actions of $\mathbb{D}_6 = \langle \rho, \sigma, \tau \rangle$ on each of the six isotypic components $V^{(j)}$ of the $\mathbb{D}_6$ action on $L^2(\Omega)$. This describes the six possibilities (barring accidental degeneracy) for the $\mathbb{D}_6$ action on the center eigenspace $E$ at a degenerate critical point.

Following [6, 10, 11], we define a *maximal isotropy subgroup* of a $\Gamma$ action on $V$ to be an isotropy subgroup $\Sigma \neq \Gamma$ with the property that if $\Theta$ is an isotropy subgroup such that $\Sigma \leq \Theta$, then $\Theta = \Sigma$ or $\Theta = \Gamma$. In other words, a maximal isotropy subgroup is a maximal proper isotropy subgroup. If $\dim(\mathrm{Fix}(\Sigma, E)) = 1$, then $\Sigma$ is a maximal isotropy subgroup of the $\Gamma$ action on $E$. The converse, however, is not true.

In gradient systems, for example the PDE (1), more can be said. If $\Sigma$ is any maximal isotropy subgroup of the $\Gamma$ action on $E$, then there is typically a solution branch created at the bifurcation with isotropy subgroup $\Sigma$. If $\dim \mathrm{Fix}(\Sigma, E) \geq 2$, the branch created is an example of a non-EBL branch. See [30] for a discussion of bifurcations in gradient systems.

By Proposition 4.5, the effective symmetry group of $\tilde{g}$, restricted to $\mathrm{Fix}(\Sigma, E)$, is $N_\Gamma(\Sigma)/\Sigma$. This effective symmetry group determines how solutions with symmetry $\Sigma$ bifurcate.

*Example* 4.12. Consider a degenerate critical point with isotropy subgroup $\Gamma_1 = \mathbb{D}_6 = \langle \rho, \sigma, \tau \rangle$. Barring accidental degeneracy, the center eigenspace $E$ is a subspace of one of the 6 isotypic components of the $\mathbb{D}_6$ action on $L^2(\Omega)$ described in Example 4.8. Figure 3 shows the lattice of isotropy subgroups for $\mathbb{D}_6$ acting on each of these 6 isotypic components $V^{(j)}$. These 6 cases can be distinguished by determining which isotypic component an arbitrary eigenfunction in $E$ belongs to. We shall go through each of these six cases, and describe the resulting bifurcation. Recall that $\Gamma = \Gamma_1 = \mathbb{D}_6$ for each of these six cases, and $\Gamma' = \mathrm{pStab}(E, \Gamma)$.

$$
\begin{aligned}
E \subseteq V^{(1)} \Rightarrow &\quad \Gamma' = \Gamma_1 = \langle \rho, \sigma, \tau \rangle, \quad \dim E = 1, \quad \Gamma/\Gamma' \cong \langle 1 \rangle \\
E \subseteq V^{(2)} \Rightarrow &\quad \Gamma' = \Gamma_{13} = \langle \rho \rangle, \qquad\quad \dim E = 1, \quad \Gamma/\Gamma' \cong \mathbb{Z}_2 \\
E \subseteq V^{(3)} \Rightarrow &\quad \Gamma' = \Gamma_9 = \langle \rho^2, \sigma \rangle, \qquad \dim E = 1, \quad \Gamma/\Gamma' \cong \mathbb{Z}_2 \\
E \subseteq V^{(4)} \Rightarrow &\quad \Gamma' = \Gamma_{10} = \langle \rho^2, \tau \rangle, \qquad \dim E = 1, \quad \Gamma/\Gamma' \cong \mathbb{Z}_2 \\
E \subseteq V^{(5)} \Rightarrow &\quad \Gamma' = \Gamma_{19} = \langle \rho^3 \rangle, \qquad\quad \dim E = 2, \quad \Gamma/\Gamma' \cong \mathbb{D}_3 \\
E \subseteq V^{(6)} \Rightarrow &\quad \Gamma' = \Gamma_{22} = \langle 1 \rangle, \qquad\quad \dim E = 2, \quad \Gamma/\Gamma' \cong \mathbb{D}_6.
\end{aligned}
$$

The first case, $E \subseteq V^{(1)} = \mathrm{Fix}(\Gamma_1, L^2(\Omega))$, does not lead to a symmetry-breaking bifurcation. The $\mathbb{D}_6$ action on $E$ is trivial, so the EBL does not apply. The degenerate critical point $(u^*, \lambda^*)$ is typically a fold point (or saddle-node), not a bifurcation point. In the neighborhood of the fold point there is only one solution branch, with isotropy subgroup $\Gamma_1$, and the branch lies to one side of $\lambda = \lambda^*$ or the other.

The next three cases, with $\Gamma/\Gamma' \cong \mathbb{Z}_2$ symmetry, are called *pitchfork bifurcations*. Clearly, the only maximal isotropy subgroup is $\Gamma'$ in each case, and the EBL applies. The effective symmetry group acting on $E$ is $\mathbb{Z}_2$, so there are two conjugate solution branches created at the bifurcation. In the branch following code we follow one of these branches using the pmGNGA starting with any eigenvector $e \in E$.

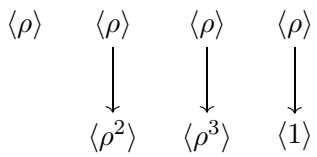


FIGURE 4. The diagrams of the four isotropy lattices for the actions of $\Gamma_{13} = \langle\rho\rangle$ on each of the four isotypic components $V^{(j)}_{\langle\rho\rangle}$ of the $\Gamma_{13}$ action on $L^2(\Omega)$. This describes the four possibilities (barring accidental degeneracy) for the $\Gamma_{13}$ action on the center eigenspace $E$ at a degenerate critical point.

The next case, with $E \subseteq V^{(5)}$, is a bifurcation with $\mathbb{D}_3$ symmetry. The maximal isotropy subgroup $\Gamma_5 = \langle\sigma, \tau\rangle$ satisfies

$$\dim \mathrm{Fix}(\Gamma_5, E) = 1, \text{ and } N_{\Gamma_1}(\Gamma_5)/\Gamma_5 = \langle 1\rangle.$$

Our branch following code uses a projection operator to find an eigenvector $e \in E$ with $\mathrm{Stab}(e, \Gamma_1) = \Gamma_5$. The pmGNGA using this eigenvector $e$ will follow one of the solution branches created at the bifurcation, and the pmGNGA using the negative eigenvector $-e$ will find a branch that is not conjugate to the first. Bifurcations with $\mathbb{D}_3$ symmetry are typically transcritical, and two $\mathbb{D}_3$-orbits of branches are created at the bifurcation [10, 11].

The last case, with $E \subseteq V^{(6)}$, is a bifurcation with $\mathbb{D}_6$ symmetry. There are two maximal symmetry types, the conjugacy classes of $\Gamma_{15}$ and $\Gamma_{16}$. A calculation shows that

$$\dim \mathrm{Fix}(\Gamma_{15}, E) = \dim \mathrm{Fix}(\Gamma_{16}, E) = 1, \text{ and } N_{\Gamma_1}(\Gamma_{15})/\Gamma_{15} = N_{\Gamma_1}(\Gamma_{16})/\Gamma_{16} = \mathbb{Z}_2.$$

To follow one branch from each of the group orbits of solution branches created at this bifurcation, it suffices to use the pmGNGA twice, with the eigenvectors $e_1, e_2 \in E$, where $\mathrm{Stab}(e_1, \Gamma_1) = \Gamma_{15}$ and $\mathrm{Stab}(e_2, \Gamma_1) = \Gamma_{16}$. It is well-known that these EBL-branches are typically the only branches created at a bifurcation with $\mathbb{D}_6$ symmetry [10, 11].

*Example* 4.13. Consider a degenerate critical point with isotropy subgroup $\Gamma_{13} = \langle\rho\rangle \cong \mathbb{Z}_6$. Barring accidental degeneracy, the center eigenspace $E$ is a subspace of one of the 4 isotypic components $V^{(j)}_{\langle\rho\rangle}$ defined in Example 4.9. Figure 4 shows the lattice of isotropy subgroups for $\Gamma_{13}$ acting on each of these 4 isotypic components. Recall that $\Gamma = \Gamma_{13} = \langle\rho\rangle$ for each of these cases, and the minimal isotropy subgroup is $\Gamma' = \mathrm{pStab}(E, \Gamma)$. We shall go through each of the four cases, and describe the resulting bifurcation:

$$\begin{aligned}
E \subseteq V^{(1)}_{\langle\rho\rangle} = V^{(1)} \oplus V^{(2)} &\Rightarrow \Gamma' = \Gamma_{13} = \langle\rho\rangle, \quad \dim E = 1, \quad \Gamma/\Gamma' \cong \langle 1\rangle \\
E \subseteq V^{(2)}_{\langle\rho\rangle} = V^{(3)} \oplus V^{(4)} &\Rightarrow \Gamma' = \Gamma_{21} = \langle\rho^2\rangle, \quad \dim E = 1, \quad \Gamma/\Gamma' \cong \mathbb{Z}_2 \\
E \subseteq V^{(3)}_{\langle\rho\rangle} = V^{(5)} &\Rightarrow \Gamma' = \Gamma_{19} = \langle\rho^3\rangle, \quad \dim E = 2, \quad \Gamma/\Gamma' \cong \mathbb{Z}_3 \\
E \subseteq V^{(4)}_{\langle\rho\rangle} = V^{(6)} &\Rightarrow \Gamma' = \Gamma_{22} = \langle 1\rangle, \quad \dim E = 2, \quad \Gamma/\Gamma' \cong \mathbb{Z}_6.
\end{aligned}$$

The first two cases are analogous to the first two cases in Example 4.12. When $\Gamma/\Gamma' \cong \langle 1\rangle$ there is a fold point, but no symmetry breaking bifurcation. There is a pitchfork bifurcation when $\Gamma/\Gamma' \cong \mathbb{Z}_2$. The next two cases are interesting because $\Gamma_{13}$ does not act absolutely irreducibly on $E$, and the EBL does not apply. In both cases $\Gamma'$ is a maximal isotropy subgroup.

In the third case, where $E \subseteq V^{(3)}_{\langle\rho\rangle} = V^{(5)}$, every eigenfunction in the 2-dimensional $E$ has isotropy subgroup $\Gamma_{19}$. Since we have a gradient system, we know that solution branches with isotropy subgroup $\Gamma_{19}$ are created at this bifurcation with $\mathbb{Z}_3$ symmetry. The bifurcation is well-understood, and it looks like a bifurcation with $\mathbb{D}_3$ symmetry, except that the "angle" of the bifurcating solutions in the $E$ plane is arbitrary. This means that trial and error is needed, in

general, to find eigenfunctions in $E$ for which the pmGNGA will converge. If a branch is found for a starting eigenfunction $e$, then the eigenfunction $-e$ is used to find the other solution branch.

In the fourth case, where $E \subseteq V^{(4)}_{\langle\rho\rangle} = V^{(6)}$, every eigenfunction in $E$ has the same isotropy subgroup: $\Gamma_{22} = \langle 1\rangle$. Gradient bifurcations with $\mathbb{Z}_6$ symmetry look like bifurcations with $\mathbb{D}_6$ symmetry, except that the angle in the $E$ plane is arbitrary. Again, trial and error is needed to find starting eigenfunctions for which the pmGNGA converges.

**The Bifurcation Digraph.** A calculation similar to those summarized in Examples 4.12 and 4.13 was done for each of the isotropy subgroups of the $\mathbb{D}_6 \times \mathbb{Z}_2$ action on $L^2(\Omega)$. The calculations were done by hand, and verified with GAP. There are 59 generic symmetry-breaking bifurcations, one for each isotypic component $V^{(j)}_{\Gamma_i}$ on which $\Gamma_i$ acts nontrivially. The amount of information is overwhelming, so we display the essential results in what we call a bifurcation digraph.

**Definition 4.14.** The *bifurcation digraph* of the $\Gamma_0$ action on a real vector space $V$ is a directed graph with labelled arrows. The vertices are the symmetry types (equivalence classes of isotropy subgroups). Given $\Sigma \le \Gamma$, two isotropy subgroups of the $\Gamma_0$ action on $V$, we draw an arrow from $[\Gamma]$ to $[\Sigma]$ iff $\Sigma$ is a maximal isotropy subgroup of the $\Gamma$ action on some isotypic component $V^{(j)}_\Gamma$ of $V$. Each arrow has the label $\Gamma/\Gamma'$, where $\Gamma'$ is the kernel of the $\Gamma$ action on $V^{(j)}_\Gamma$. Furthermore, each arrow is either solid, dashed or dotted. The arrow is

$$\begin{aligned} \text{solid if } &\dim \mathrm{Fix}(\Sigma, E) = 1 \text{ and } N_\Gamma(\Sigma)/\Sigma = \mathbb{Z}_2, \\ \text{dashed if } &\dim \mathrm{Fix}(\Sigma, E) = 1 \text{ and } N_\Gamma(\Sigma)/\Sigma = \langle 1\rangle, \text{ and} \\ \text{dotted if } &\dim \mathrm{Fix}(\Sigma, E) \ge 2, \end{aligned}$$

where $E$ is any irreducible subspace contained in $V^{(j)}_\Gamma$.

Note that if $\dim \mathrm{Fix}(\Sigma, E) = 1$, then $N_\Gamma(\Sigma)/\Sigma$ is either $\mathbb{Z}_2$ or $\langle 1\rangle$, since these are the only linear group actions on $E \cong \mathbb{R}^1$. Thus, the three arrow types (solid, dashed, and dotted) exhaust all possibilities.

**Theorem 4.15.** *For a given $\Gamma_0$ action on $V$, every arrow in the diagram of the isotropy lattice is an arrow in the bifurcation digraph.*

*Proof.* Suppose $[\Gamma] \to [\Sigma]$ is an arrow in the diagram of the isotropy lattice. Then some $\Sigma^* \in [\Sigma]$ is a maximal isotropy subgroup of the $\Gamma$ action on $V$. Choose $u^* \in V$ such that $\mathrm{Stab}(u^*, \Gamma) = \Sigma^*$. Such a $u^*$ exists since $\Sigma^*$ is an isotropy subgroup. Now consider the isotypic decomposition $\{V^{(j)}_\Gamma\}_{j\in J}$ of $V$. We can write $u^* = \sum_{j\in J} u^{(j)}$, where $u^{(j)} \in V^{(j)}_\Gamma$ are uniquely determined. Let $\gamma$ be any element of $\Sigma^*$. Then $\gamma \cdot u^* = \sum_{j\in J} \gamma \cdot u^{(j)} = u^*$. Since each of the components $V^{(j)}_\Gamma$ is $\Gamma$-invariant, $\gamma \cdot u^{(j)} = u^{(j)}$ for each $j \in J$. Thus $\Sigma^* \le \mathrm{Stab}(u^{(j)}, \Gamma)$ for each $j \in J$. Either $\mathrm{Stab}(u^{(j)}, \Gamma) = \Gamma$ or $\mathrm{Stab}(u^{(j)}, \Gamma) = \Sigma^*$, since $\Sigma^*$ is a maximal isotropy subgroup of the $\Gamma$ action on $V$. If $\mathrm{Stab}(u^{(j)}, \Gamma) = \Gamma$ for all $j \in J$, then $\mathrm{Stab}(u^*, \Gamma) = \Gamma$. But $\mathrm{Stab}(u^*, \Gamma) \ne \Gamma$, so $\mathrm{Stab}(u^{(j)}, \Gamma) = \Sigma^*$ for some $j \in J$, and $\Sigma^*$ is a maximal isotropy subgroup of the $\Gamma$ action on this component $V^{(j)}_\Gamma$ of $V$. Therefore the bifurcation digraph has an arrow from $[\Gamma]$ to $[\Sigma^*] = [\Sigma]$. □

Theorem 4.15 says that the bifurcation digraph is an extension of the diagram of the isotropy lattice. The bifurcation digraph has more arrows, in general. As with the lattice of isotropy subgroups, we usually draw a single element $\Gamma$ of the equivalence class $[\Gamma]$ for each vertex of the bifurcation digraph.

An arrow from $\Gamma$ to $\Sigma$ in the bifurcation digraph indicates that a $\Gamma_0$-equivariant gradient system $g(\lambda, u) = 0$ can have a generic symmetry-breaking bifurcation where a mother branch with isotropy subgroup $\Gamma$ creates a daughter branch with isotropy subgroup $\Sigma$. The symmetry group of the bifurcation is $\Gamma/\Gamma'$, and the center eigenspace at the bifurcation point is the $\Gamma$-irreducible space

$E$. The information encoded in the label and arrow type is used by the heuristics of our branch-following algorithm. A solid arrow indicates that every $e$ in the one-dimensional space $\mathrm{Fix}(\Sigma, E)$ satisfies $\gamma \cdot e = -e$ for some $\gamma \in \Sigma$. Thus, there is typically a pitchfork bifurcation in the space $\mathrm{Fix}(\Sigma, E)$. A dashed arrow indicates that $\gamma \cdot e = e$ for all $e \in \mathrm{Fix}(\Sigma, E)$ and $\gamma \in \Sigma$. Thus, the daughter branches bifurcating in the directions $e$ and $-e$ are not conjugate. A dotted arrow indicates that the EBL does not apply to this bifurcation. As mentioned above, branching of solutions corresponding to a dotted arrow is generic in gradient systems [30, 10].

A condensed bifurcation digraph for the $\mathbb{D}_6 \times \mathbb{Z}_2$ action on $L^2(\Omega)$ is shown in Figure 5. The calculations for the directed edges coming from $\Gamma_1$ and $\Gamma_{13}$ are described in examples 4.12 ane 4.13, respectively. The digraph has 65 directed edges, but there are only 5 possibilities for the symmetry group of the bifurcation: $\Gamma/\Gamma' = \mathbb{Z}_2$, $\mathbb{Z}_3$, $\mathbb{Z}_6$, $\mathbb{D}_3$, or $\mathbb{D}_6$. The symmetry-breaking bifurcation with each of these symmetries is well understood [10, 11], and each is described briefly in Example 4.12 or 4.13. This digraph is of great help in writing an automated code for branch following.

In our problem the label $\Gamma/\Gamma'$ and arrow type are sufficient to characterize the bifurcation completely. For more complicated groups, the label may need to contain more information about the action of $\Gamma$ on $E$. For example the label $\Gamma/\Gamma' = \mathbb{S}_4$ would be ambiguous, since $\mathbb{S}_4$ has two faithful irreducible representations with different lattices of isotropy subgroups.

## 5. Symmetry and Computational Efficiency.

Several modifications of the GNGA (2.1) take advantage of symmetry to speed up the calculations. The symmetry forces many of the components of the gradient and Hessian to be zero. We identified these zero components and avoided doing the time-consuming numerical integrations to compute them. At the start of the C++ program, the isotropy subgroup, $\Gamma_i$, of the initial guess is computed. Recall that there are $M$ modes in the Galerkin space $B_M$, so $\dim(B_M) = M$. Define $M_i := \dim(\mathrm{Fix}(\Gamma_i, B_M))$. We chose the representatives $\Gamma_i$ within each conjugacy class so that $\mathrm{Fix}(\Gamma_i, B_M)$ is a coordinate subspace of $B_M$. Thus, $M - M_i$ components of the gradient $g(\lambda, u)$ are zero if $\mathrm{Fix}(u) = \Gamma_i$. The numerical integrations in (5) are done only for the $M_i$ potentially nonzero components of $g$. Similarly, $M_i(M_i + 1)/2$ rather than $M(M + 1)/2$ numerical integrations are needed to compute the part of the Hessian matrix $h$ needed by the GNGA algorithm: The numerical integrations in (6) are done only if $\psi_j$ and $\psi_k$ are both in $\mathrm{Fix}(\Gamma_i, B_M)$. The system $h\chi = g$ for the Newton step $\chi$ reduces to a system of $M_i$ equations in $M_i$ unknowns. After Newton's method converges to a solution, the full Hessian needs to be calculated in order to compute the MI. Here, too, we can take advantage of the symmetry: Since $h$ is $\Gamma_i$-equivariant, $h_{jk} = 0$ if $\psi_j$ and $\psi_k$ are in different isotypic components $V_{\Gamma_i}^{(j)}$ of $B_M$.

As an example, consider the execution time for approximating a solution with $\Gamma_1$ symmetry using $M = 300$ modes and a level $\ell = 5$ grid on a 1GHz PC. Our C++ code uses only $M_1 = 30$ modes, and takes about 1.5 seconds per Newton step, compared to 44 seconds when the symmetry speedup is not implemented.

## 6. Automated Branch Following.

The branch following code is a complex collection of about a dozen Perl scripts, *Mathematica* and Gnuplot scripts, and a C++ program. These programs write and call each other fully automatically and communicate through output files, pipes and command line arguments. A complete bifurcation diagram can be produced by a single call to the main Perl script.

Two choices for the function of $u$ plotted vs. $\lambda$ are shown in Figure 6. In most bifurcation diagrams we plot approximate solutions $u$ evaluated at a generic point $(2/27, 4\sqrt{3}/27)$ (the big dot in Figure 1) versus the parameter $\lambda$; other choices for the vertical axis such as $J(u)$ or $\|u\|_\infty$ lead to less visible separation of branches. Two conjugate solutions can have different values at the generic point, but since our program follows only one branch in each group orbit this does not cause a problem.

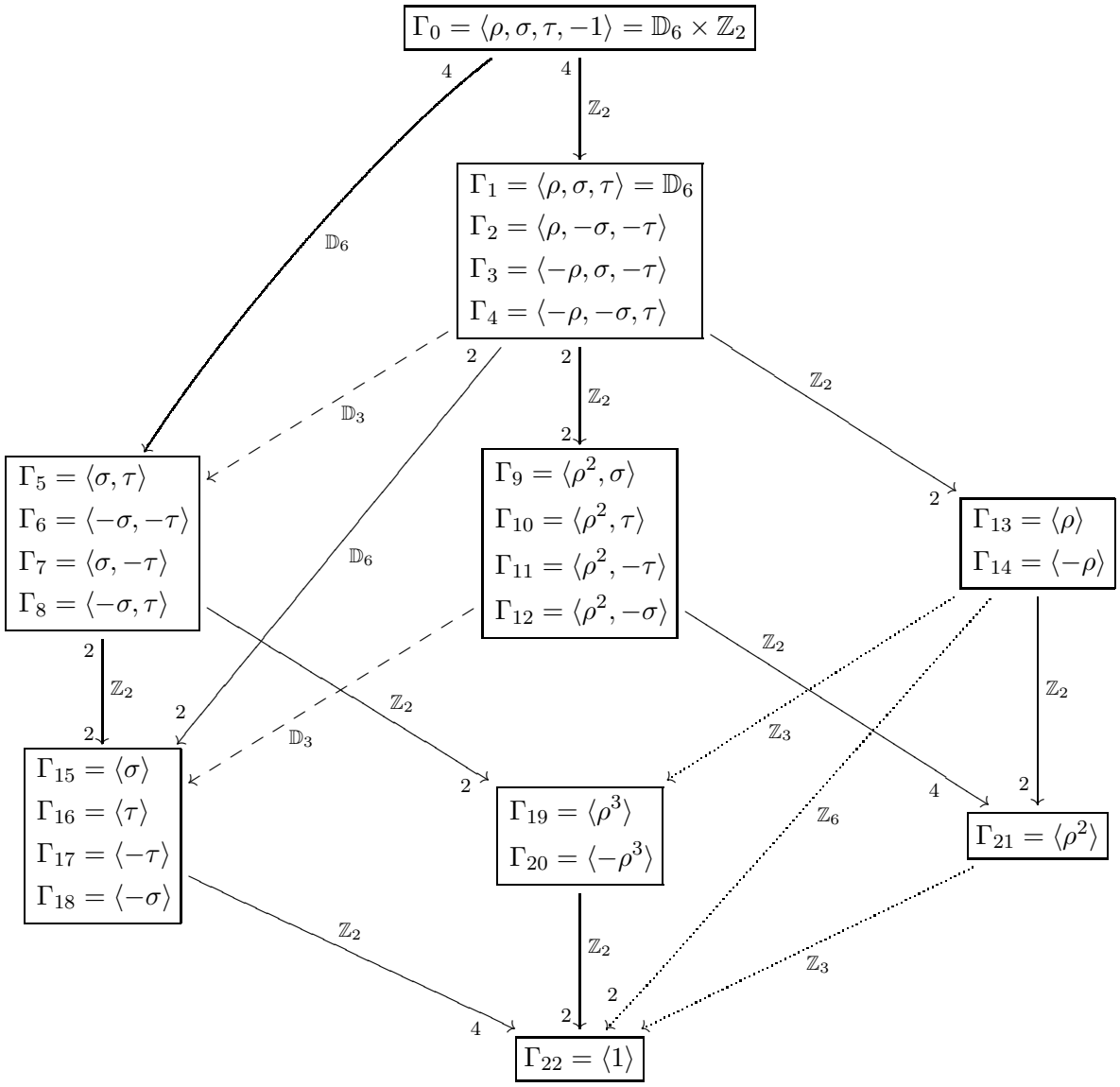


FIGURE 5. The bifurcation digraph for the $\mathbb{D}_6 \times \mathbb{Z}_2$ action on $L^2(\Omega)$ extends the diagram of the isotropy lattice. The digraph shown is condensed as in Figure 2. The arrows indicate generic symmetry breaking bifurcations. The Morse index of the mother branch changes by 1 at bifurcations with $\mathbb{Z}_2$ symmetry, and it changes by 2 at all other bifurcations shown here.

The C++ program implements the GNGA algorithm. Its input is a vector of coefficients $a \in \mathbb{R}^M$ for an initial guess in Newton's method, an interval for $\lambda$, a stepsize for $\lambda$ and several other parameters such as the grid level. It finds solutions on a single branch of the bifurcation diagram. Every solution is written as a single line in an output file. This line contains all the information about the solution, and can be used to write an input file for a subsequent call to the same C++ program.

The C++ program finds one branch (referred to as the main branch) and a short segment of each of the daughter branches created at bifurcations of the main branch. The coefficients approximating the first solution on the branch are supplied to the C++ program. Newton's method is used to find this first solution, then $\lambda$ is incremented and the next solution is found. The program attempts to follow the main branch all the way to the final $\lambda$, usually 0. Heuristics are used to double or halve

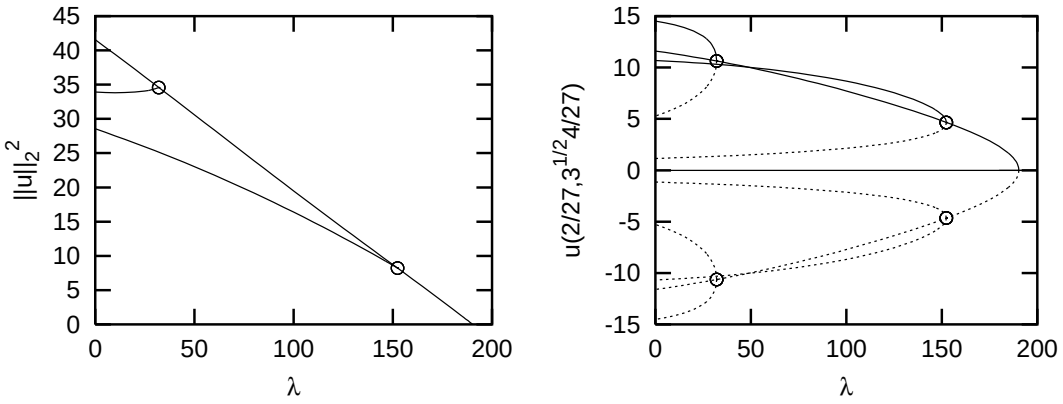


FIGURE 6. Bifurcation diagrams of the sixth primary branch (which bifurcates from $\lambda_6$), showing $||u||_2^2$ and $u(2/27, 4\sqrt{3}/27)$ as a function of $\lambda$. Since $||u||_2^2$ is a $\mathbb{D}_6 \times \mathbb{Z}_2$-invariant function of $u$, each group orbit of solution branches is shown as one curve on the left. The disadvantage of plotting $||u||_2^2$ is that the curves in many bifurcation diagrams are not well separated. The point $(2/27, 4\sqrt{3}/27)$ is not on any of the reflection axes of the snowflake region. There are 2 primary branches with symmetry $S_1$, four secondary branches with symmetry $S_9$, and four secondary branches with symmetry $S_{10}$. Our choice for the bifurcation diagrams in this paper combines the advantages of both views: $u(2/27, 4\sqrt{3}/27)$ is plotted as a function of $\lambda$ for exactly one branch (the solid lines) from each group orbit. Unless indicated otherwise, all figures were produced with level $\ell = 5$ and $M = 300$ modes.

the $\lambda$ stepsize when needed, keeping the stepsize in the interval from the initial stepsize (input to the C++ program) to 1/32 of the initial stepsize. For example, the stepsize is halved if Newton's method does not converge, if it converges to a solution with the wrong symmetry, or if more than one bifurcation is detected in one $\lambda$ step.

The Morse index is computed at each $\lambda$ value on the main branch. When the MI changes a subroutine is called to handle the bifurcation before the main branch is continued. If the MI changes from $m_1$ to $m_2$, we define $m = \max\{m_1, m_2\}$. Then the bifurcation point is approximated by using the secant method to set the $m$-th eigenvalue of the Hessian $h(u)$ to zero as a function of $\lambda$. The GNGA is needed at each step of the secant method to compute $u = u(\lambda)$. We find that the GNGA works well even though we are approximating a solution for which the Hessian is singular.

After the bifurcation point is approximated, a short segment of each bifurcating branch is computed and one output file is written for each branch, using Algorithm 6.1. If the Equivariant Branching Lemma (EBL) holds, then we know exactly which critical eigenvector to use for each branch.

*Algorithm* 6.1. (`follow_branch`)

(1) Input: bifurcation point $(\lambda, a)$, one critical eigenvector $e \in \mathbb{R}^M$, and stepsize $\Delta\lambda < 0$. Output: A file is written for one daughter branch.
(2) Write $(\lambda, a)$ to output file. Set $t = 0.1$. Set $\lambda_b = \lambda$.
(3) Compute index $k$ so that $|e_k| \geq |e_i|$ for all $i \in \{1, \ldots, M\}$.
(4) Repeat until $\lambda_b - \lambda < \Delta\lambda$, or $t < 0.1/32$ or some maximum number of points have been written to the file.
    (a) Do the pmGNGA with initial guess $(\lambda, a + t\,e)$, fixing coefficient $k$.
    (b) If Newton's method converges replace $(\lambda, a)$ by the solution found and write this point to the file, else $t \leftarrow t/2$.

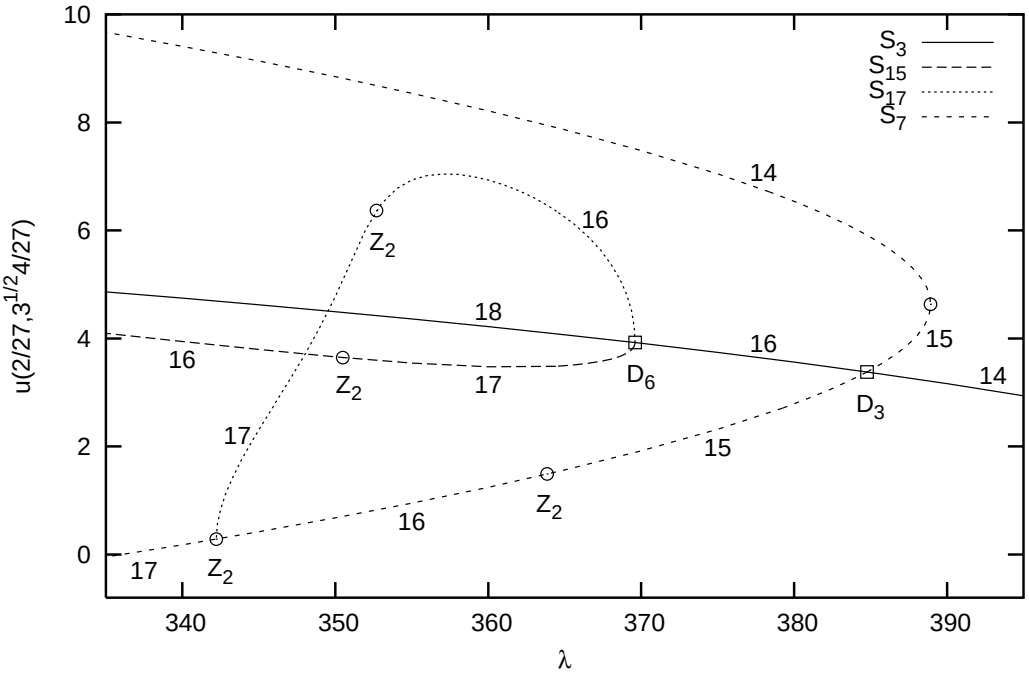


FIGURE 7. A partial bifurcation diagram of the 14-th primary branch showing a $\mathbb{D}_6$, a $\mathbb{D}_3$ and several $\mathbb{Z}_2$ bifurcations. At the $\mathbb{D}_6$ bifurcation, 12 branches in two different group orbits are born. In accordance with Figure 6, only two branches are followed and shown on this bifurcation diagram. An animation showing the followed branch with symmetry type $S_{15}$ is shown in `s3s15.gif`, and an animation of the followed branch with symmetry type $S_{17}$ is in `s3s17s7.gif`. Note that this branch with $S_{17}$ symmetry "dies" at a bifurcation with $\mathbb{Z}_2$ symmetry, showing that we cannot always make a consistent distinction between secondary and tertiary branches. At the $\mathbb{D}_3$ bifurcation, 6 branches in two different group orbits are born. As before, only two branches are followed. An animation showing the "upper" branch with symmetry type $S_7$, through the bifurcation point and continuing to the "lower" branch with symmetry type $S_7$ is shown in `s7s3s7.gif`. For clarity, the branches bifurcating from 3 of the $\mathbb{Z}_2$ bifurcations are not shown. The numbers next to a branch indicate the MI of the solution. The MI changes by 2 at a square, and by 1 at a circle.

Note that the pmGNGA can follow a branch that bifurcates to the right or the left. Those that bifurcate to the right usually turn over in a saddle-node "bifurcation" that does not offer any difficulty for the pmGNGA. Figures 7 and 8 show several examples of bifurcations.

The EBL does not hold at bifurcations with $\mathbb{Z}_3$ and $\mathbb{Z}_6$ symmetry in our problem, since the 2-dimensional center eigenspace does not have a 1-dimensional subspace with more symmetry. Figure 8 shows one of the few bifurcations with $\mathbb{Z}_3$ symmetry that we observed. By good fortune, the branches with symmetry type $S_{19}$ were successfully followed using the same eigenvectors one would choose for a bifurcation with $\mathbb{D}_3$ symmetry. A better method for following bifurcating solutions that are not predicted by the EBL would be to use the pmGNGA with random (normalized) eigenvectors in $E$ repeatedly until it appears that all equivalence classes of solutions have been found.

The branch following code is called recursively by a main Perl script. Initially, the C++ program follows the trivial branch on a given $\lambda$ range. This results in an output file for the trivial branch and another output file for each bifurcating primary branch. Then the short parts of the primary branches are followed with more calls to the C++ program. Any bifurcating branch results in a new output file, and the Perl script makes another call to the C++ program to continue that

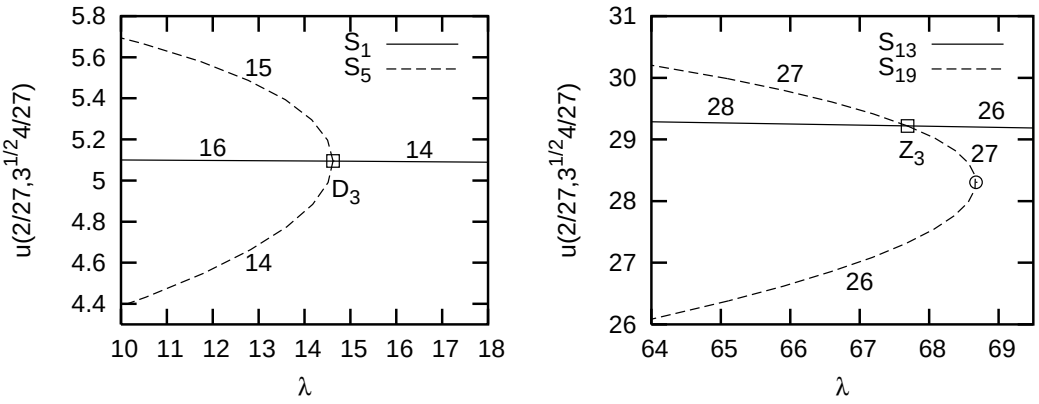


FIGURE 8. The $\mathbb{D}_3$ bifurcation of the 13-th primary branch is on the left. This is the only observed $\mathbb{D}_3$ bifurcation that is not transcritical. An animation of the upper branch with symmetry type $S_5$, through the bifurcation point and continuing with the lower branch is shown in `s5s1s5.gif`. A $\mathbb{Z}_3$ bifurcation of a daughter of the 24-th primary branch is shown on the right. The branches created at this bifurcation are not described by the EBL. An animation of the branches with symmetry type $S_{19}$ is shown in `s19s13s19.gif`.

branch. The main Perl script's most important job is book keeping. It saves the output files with distinct names, and calls the branch following code to continue each of the new branches. The process stops when all the branches are fully followed within the given $\lambda$ range.

In this way, a complete bifurcation diagram is produced by a single invocation of the main Perl script. There is no need to guess initial conditions for input to Newton's method, since the trivial solution is known exactly ($a = 0$) and all the other solutions are followed automatically.

The main Perl script calls several other smaller scripts. For example, there is a script which extracts solutions from output files and feeds them to the branch following code as input. Another script creates Gnuplot scripts on the fly to generate bifurcation diagrams. Perl scripts are used to automatically number and store the output files and create human readable reports about them.

## 7. Numerical Results.

Our goal was to find solutions to (1, 2) at $\lambda = 0$ with each of the 23 symmetry types. The 24-th primary branch is the first one with symmetry type $S_2$, so we followed the first 24 primary branches. With level $\ell = 5$ and $M = 300$ modes, which gave our most accurate results, this found solutions with all symmetry types except $S_{11}$ and $S_{14}$. We then searched the first 100 primary branches, only following solutions with symmetry above $S_{11}$ and $S_{14}$ on the bifurcation digraph (Figure 5.) In this way we found solutions with all 23 symmetry types. The bifurcation diagrams which lead to these solutions are shown in Figures 9–12. We chose one solution at $\lambda = 0$ with each symmetry type by taking the one descended from the lowest primary branch. These choices are indicated by dots in Figures 9–12, and the corresponding contour diagrams of the solutions are shown in Figures 13 and 14. The contour diagrams use white for $u > 0$ and black for $u < 0$, and gray indicates $u = 0$. Equally spaced contours are drawn along with dots for local extrema. Details about the technique for generating these contour diagrams are found in [27].

We ran our experiments using a range of modes and levels in order to observe convergence and qualitative stability of the implementation of our algorithm. At level $\ell = 5$ we have computed 300 eigenfunctions so $M \leq 300$ is possible. At level $\ell = 6$ we computed only 100 eigenfunctions. Due to our limited computational resources, using more than 100 modes on level 6 was not practical.

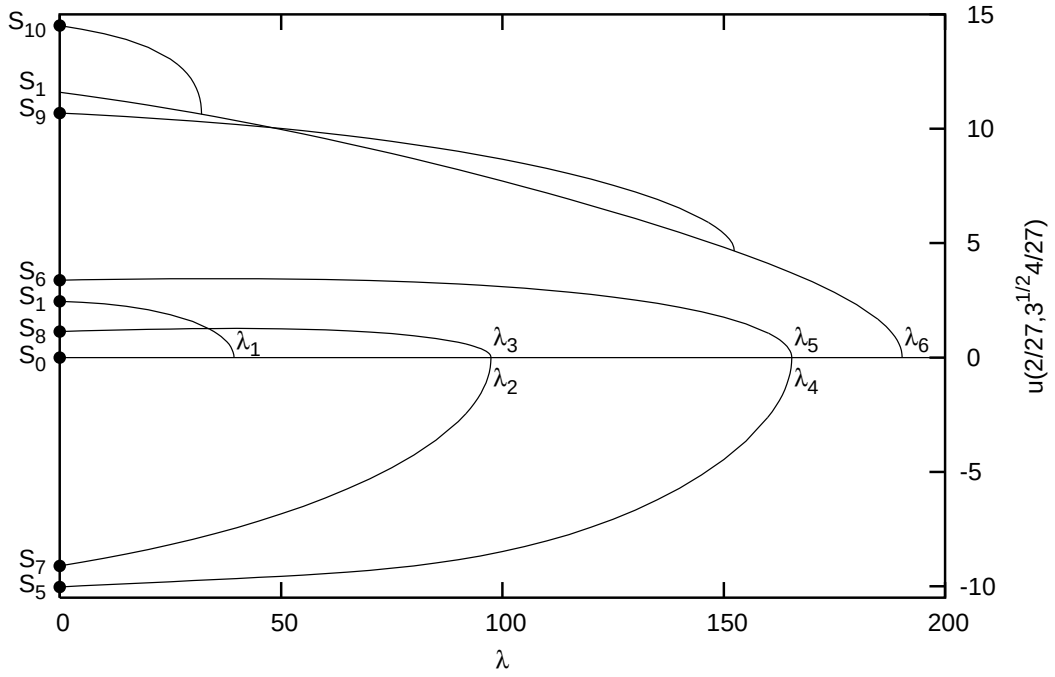


FIGURE 9. The complete bifurcation diagram for the first six primary branches bifurcating from the trivial branch. The second branch, with symmetry $S_7$, contains the CCN solution. The dots at $\lambda = 0$ in Figures 9–12 correspond to solutions depicted in Figures 13 and 14. We used the level 5 grid with 300 modes in creating all bifurcation diagrams. In Figure 15 convergence data for the solution of symmetry type $S_{10}$ at $\lambda = 0$ is provided.

As an indication of the convergence, consider the bifurcation diagram in Figure 9. The diagram looks qualitatively the same for any choice of $\ell$ and $M$ that we used. The position of the bifurcation point creating the $S_{10}$ solution (near $\lambda = 30$) changes slightly, according to this table:

| | $\ell = 4$ | $\ell = 5$ | $\ell = 6$ |
|---|---|---|---|
| $M = 100$ | 35.3931 | 34.9814 | 34.9252 |
| $M = 200$ | 32.1131 | 32.2964 | |
| $M = 300$ | | 32.0518 | |

.

The level 5 and 6 approximations with $M = 100$ modes are very close, but increasing the mode number has more of an effect. This indicates that the results with $(\ell, M) = (5, 300)$ are more accurate than those with $(6, 100)$. Figure 15 shows how $u(2/27, 4\sqrt{3}/27)$ varies with mode number and $\ell$ for the solution with $S_{10}$ symmetry at $\lambda = 0$ shown in Figures 9 and 13. The horizontal segments of the graphs correspond to the addition of modes with zero coefficients for this solution. Based on this and other similar convergence results, we chose to use level 5 with 300 modes in most of our numerical experiments.

## 8. Conclusions.

We are currently working on a more general program for recursive branch following in symmetric systems. Starting with any graph, the analog to Equation 1 is the Partial *difference* Equation (PdE) $Lu + f(u) = 0$ [25], where $L$ is the well-known discrete Laplacian on that graph and $u$ is a real-valued function on the vertices. Discretizing a PDE as we have done in this paper leads to a PdE on a graph with a large number of vertices. The grid points are the vertices of the graph, and the edges of the graph connect nearest neighbor grid points. Starting with an arbitrary graph,

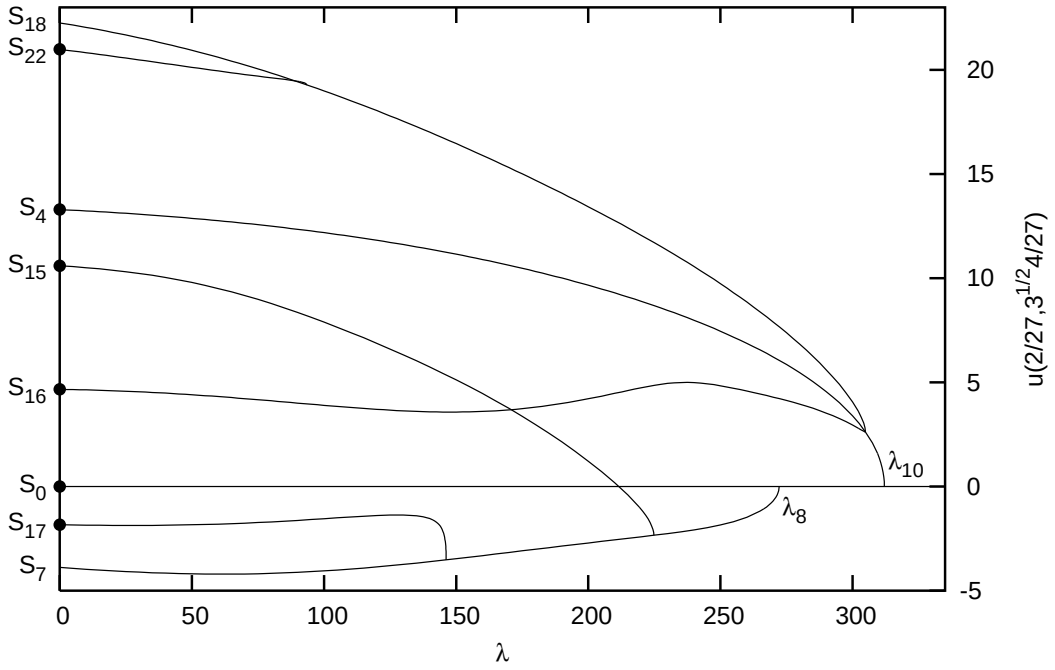


FIGURE 10. A partial bifurcation diagram showing some of the solutions bifurcating from the 8-th and 10-th primary branches. Again, the dots at $\lambda = 0$ indicate solutions shown in Figures 13 and 14. The contour plots as a function of $\lambda$ are animated for the branches ending with the dots indicating symmetry types $S_{15}$ (`s7s15.gif`), $S_{17}$ (`s7s17.gif`), $S_{16}$ (`s4s16.gif`), and $S_{22}$ (`s4s18s22.gif`).

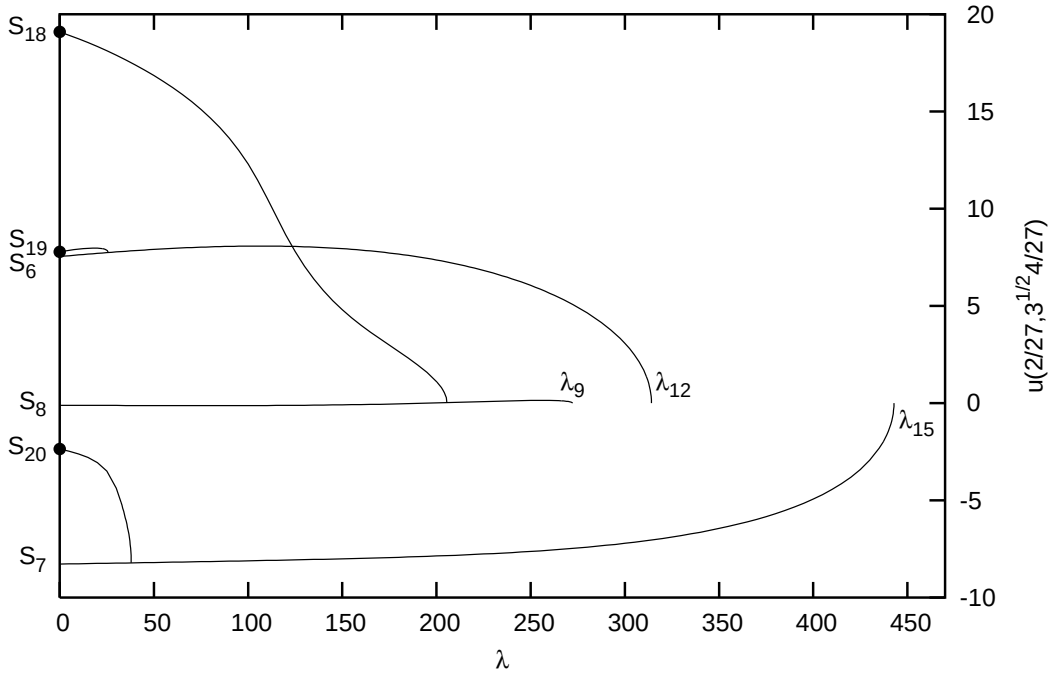


FIGURE 11. A partial bifurcation diagram providing three additional symmetry types. For clarity, the trivial branch is not shown in this and the next figure.

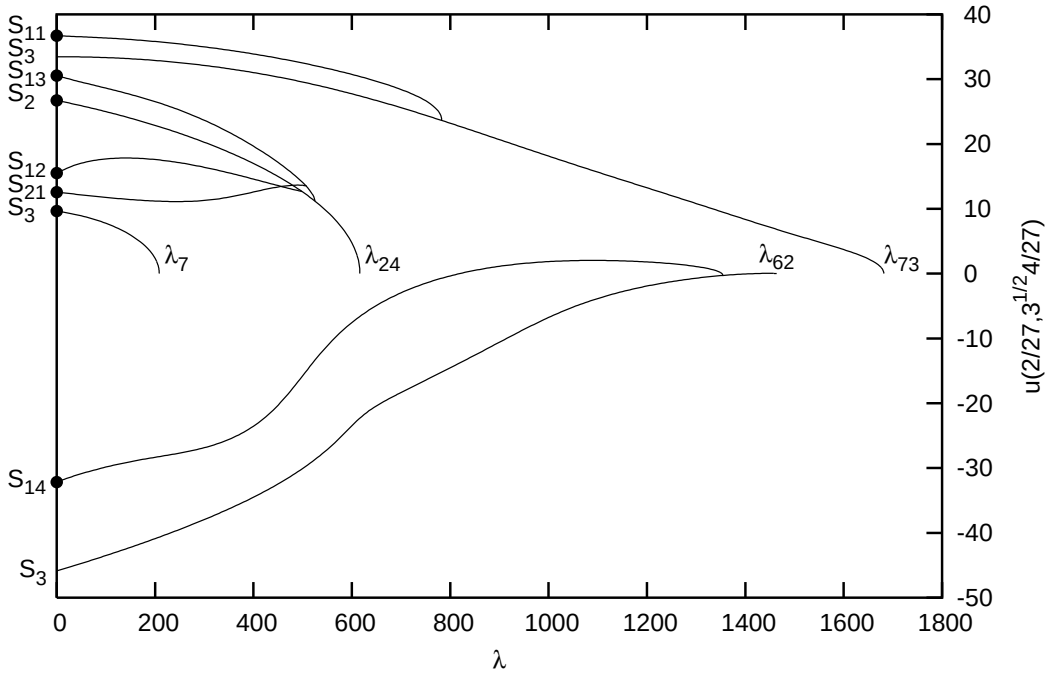


FIGURE 12. A partial bifurcation diagram containing solutions of the seven remaining symmetry types. Primary branch 24 is the first branch with symmetry type $S_2$. The symmetry types $S_{14}$ and $S_{11}$ were found by searching the first one hundred primary branches, following only those branches which can lead to solutions with the desired symmetry. These two solutions are included for completeness, but their existence for the PDE would have to be confirmed with more modes and a higher level approximation of the eigenfunctions.

our new suite of programs will analyze the symmetry of the graph and compute the bifurcation diagrams for the PdE on the graph.

The programs we describe in the current paper will work with other superlinear odd $f$ and other regions with hexagonal symmetry. The nonlinearity $f$ needs to be superlinear since our program assumes that the branches eventually "go to the left." Our general program will not have this restriction; the GNGA and pmGNGA will be replaced by a single method of branch following that is able to go through fold points, and has no prejudice about the parameter increasing or decreasing. This new method of branch following has already been successfully implemented in [33]. We hope to write the new code so that a cluster of computers can be used in parallel, with each computer following a single branch at one time, under the control of a central PERL script.

With minor modifications, our program would analyze the PDE (1) even when $f$ is not odd. The appropriate bifurcation digraph for $\mathbb{D}_6$ acting on $L^2(\Omega)$ is a subgraph of the digraph in Figure 5, so the bifurcating branches would be followed properly unless the symmetry of the mother solution is incorrectly identified. The Perl scripts which start with the trivial branch would have to be modified, since $u = 0$ is not a solution when $f$ is not odd (unless $f(0) = 0$). If $f(0) = 0$, the trivial branch exists, but its bifurcations are not properly described by the bifurcation digraph in Figure 5, and some special code would be needed to handle these bifurcations.

It is valid to ask the question "does the GNGA converge" (as implemented in this current research). While we do not have a complete proof affirming the positive of this conjecture, many references contain relevant theorems. The GNGA is an implementation of Newton's method, which indeed converges under standard assumptions. In [14], one finds the classical fixed point iteration proof that Newton's method in $\mathbb{R}^N$ converges when the initial guess is sufficiently close to a

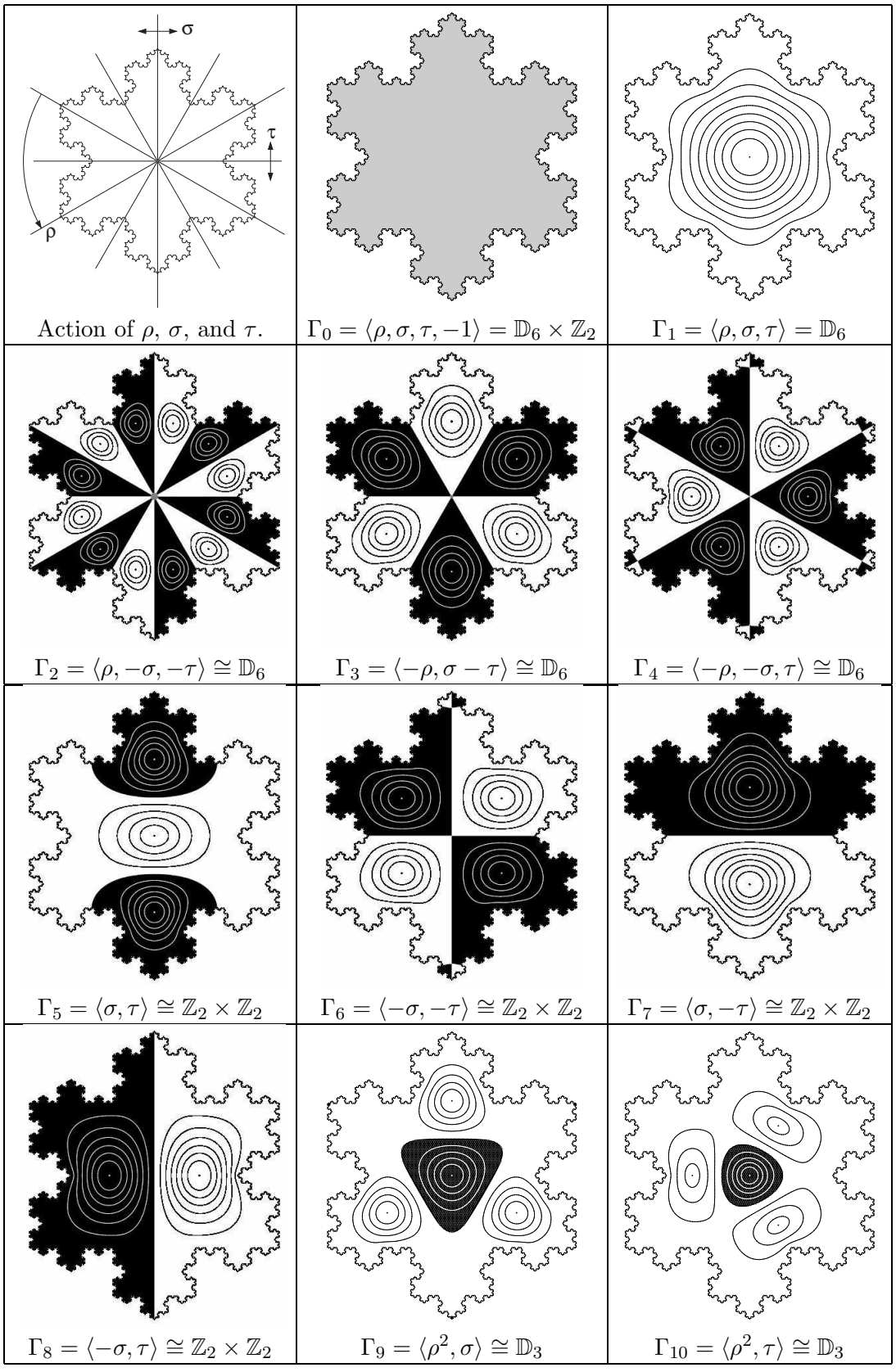


FIGURE 13. The action of the generators of $\mathbb{D}_6$ on the plane, along with contour plots of solutions with symmetry types $S_0, \ldots, S_{10}$ at $\lambda = 0$. Recall that $S_i = [\Gamma_i]$.

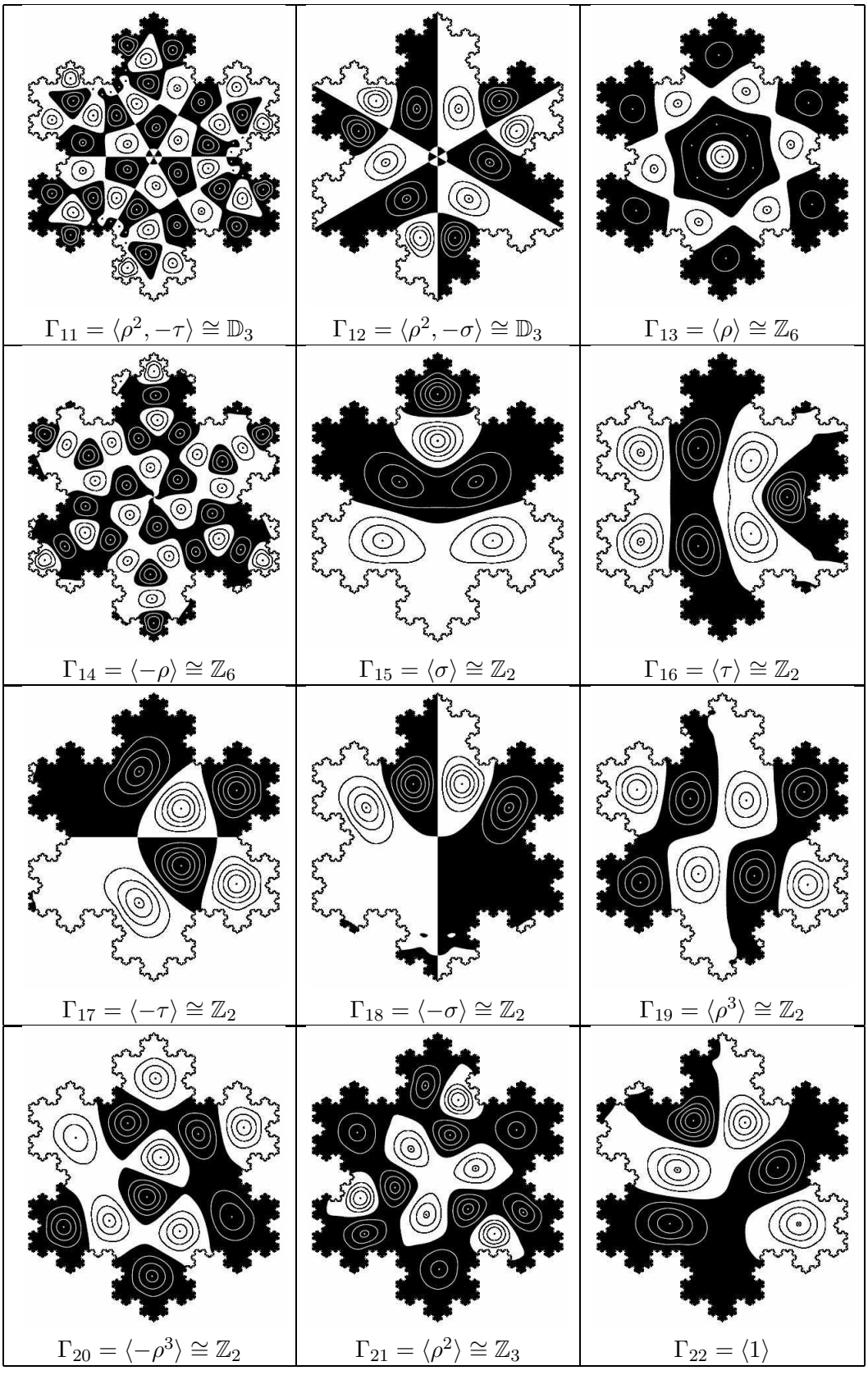


FIGURE 14. Contour plots of solutions with symmetry types $S_{11}, \ldots, S_{22}$ at $\lambda = 0$.

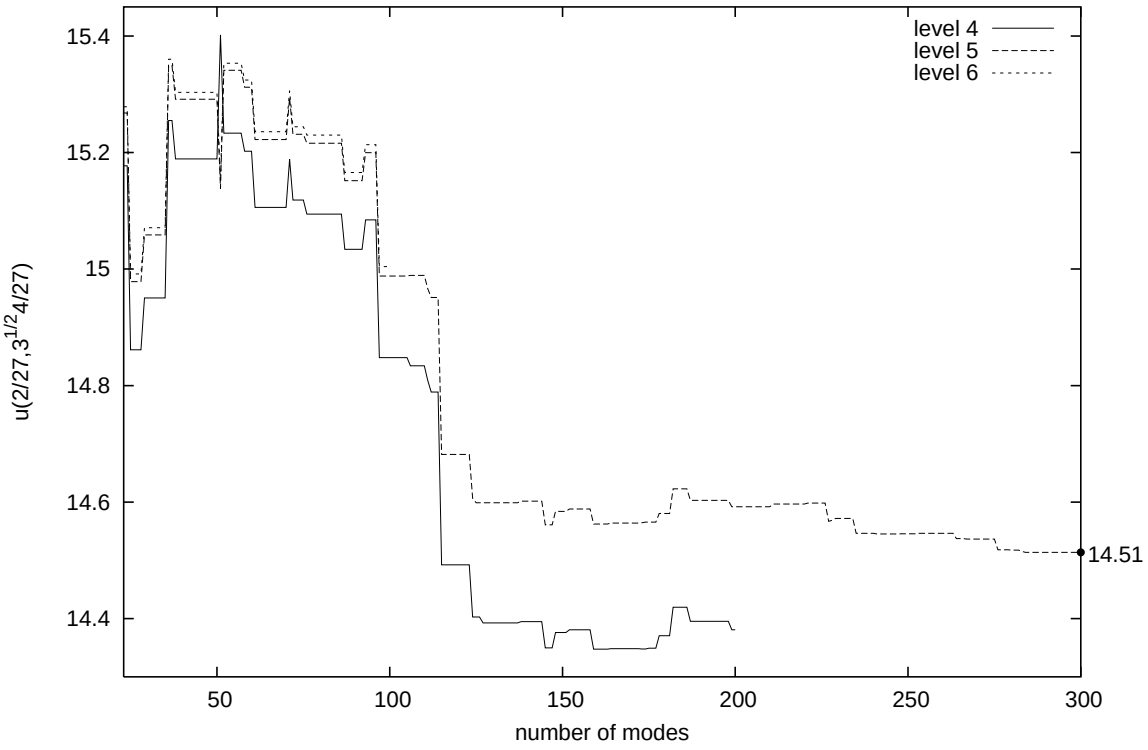


FIGURE 15. A plot of $u(2/27, 4\sqrt{3}/27)$ as a function of the number of modes for the lowest energy solution at $\lambda = 0$ with symmetry type $S_{10}$. The point at $M = 300$ matches the point labelled with $S_{10}$ in Figure 9.

nondegenerate zero of the object function. This proof applies almost without change to the infinite dimensional case. Also addressed in [14] are algorithms where the object function and/or its derivative are only approximated; this would apply to our implementation due to numerical integration errors, as well as owing to our imperfect knowledge of the eigenfunctions and corresponding eigenvalues. While not discussed exactly in the cited literature, elementary fixed point arguments indicate that the restriction of our object function $\nabla J$ to sufficiently large subspaces $B_M$ will still result in convergent iterations. It would be worthwhile to string these type of results together in order to obtain a "best possible" GNGA convergence theorem. Monograph [13] gives an easy introduction into some of the details of implementing Newton's method to solve nonlinear problems. Further, in the spirit of [7] and [35], by the invariance of the Newton map, any convergence result should hold in fixed point subspaces corresponding to a given symmetry type. The articles [20, 35] and others by those authors discuss the convergence of algorithms similar to the GNGA, at times also considering symmetry restrictions. Finally, the well-known book [3] contains relevant convergence results for Newton and approximate Newton iterative fixed point algorithms.

In summary, we have written a suite of programs that automatically computes the bifurcation diagram of the PDE (1, 2). The program finds solutions with each of the 23 symmetry types by following solution branches which are connected to the trivial branch by a sequence of symmetry-breaking bifurcations. A thorough understanding of the possible symmetry-breaking bifurcations is required for this task. We introduced the bifurcation digraph, which summarizes the results of the necessary symmetry calculations. For the group $\mathbb{D}_6 \times \mathbb{Z}_2$, these calculations were done by hand and verified by the GAP computer program [8, 21]. In the future, we plan to implement automated branch following in systems where the symmetry group is so complicated that GAP is necessary.

## References


[1] Adams, R. A., *Sobolev spaces*, Pure and Applied Mathematics, **65**. Academic Press, New York-London, 1975. xviii+268 pp.

[2] Ambrosetti, A. and P. H. Rabinowitz, *Dual variational methods in critical point theory and applications*, J. Functional Analysis **14**, pp. 349–381 (1973).

[3] Berger, M. S. *Nonlinearity and functional analysis. Lectures on nonlinear problems in mathematical analysis*, Pure and Applied Mathematics. Academic Press [Harcourt Brace Jovanovich, Publishers], New York-London, 1977. xix+417 pp.

[4] Castro, A., J. Cossio and J. M. Neuberger, *Sign-Changing Solutions for a Superlinear Dirichlet Problem*, Rocky Mnt. J. Math **27**, no. 4, pp. 1041–1053 (1997).

[5] Castro, A., P. Drabek and J. M. Neuberger, *Sign-Changing Solutions for a Superlinear Dirichlet Problem, II*, Proceedings of the Fifth Mississippi State Conference on Differential Equations and Computational Simulations, EJDE **10** (2003).

[6] Chossat, P. and R. Lauterbach, *Methods in Equivariant Bifurcations and Dynamical Systems*, Advanced Series in Nonlinear Dynamics **15**. World Scientific Publishing Co., Inc., River Edge, NJ, 2000. xvi+404 pp.

[7] Costa, D., Z. Ding and J. M. Neuberger, *A Numerical Investigation of Sign-Changing Solutions to Superlinear Elliptic Equations on Symmetric Domains*, J. Comput. Appl. Math. **131**, no. 1-2, pp. 299–319 (2001).

[8] GAP Group, *GAP – Groups, Algorithms, and Programming,* 2002, `http://www.gap-system.org`.

[9] Gilbarg, D. and N. Trudinger, *Elliptic Partial Differential Equations of Second Order*. Reprint of the 1998 edition. Classics in Mathematics. Springer-Verlag, Berlin, 2001. xiv+517 pp.

[10] Golubitsky, M., I. Stewart and D. G. Schaefer, *Singularities and Groups in Bifurcation Theory, Volume 2*, Applied Mathematical Sciences **69** Springer-Verlag, New York, 1988. xvi+533 pp.

[11] Golubitsky, M. and I. Stewart *The Symmetry Perspective: from Equilibrium to Chaos in Phase Space and Physical Space*, Progress in Mathematics **200**, Birkhäuser Verlag, Basel, 2002. xviii+325pp.

[12] Hineman, J. and J. M. Neuberger, *Numerical Solutions to Semilinear Elliptic BVP on Bunimovich Stadia*, to appear, Comm. Nonlin. Sci. Num. Sim. (2005).

[13] Kelley, C. T. *Solving Nonlinear Equations with Newton's Method. Fundamentals of Algorithms*, Society for Industrial and Applied Mathematics (SIAM), Philadelphia, PA, 2003. xiv+104 pp.

[14] Kelley, C. T. *Iterative Methods for Optimization. Frontiers in Applied Mathematics*, **18** Society for Industrial and Applied Mathematics (SIAM), Philadelphia, PA, 1999. xvi+180 pp.

[15] Lapidus, M., *Fractal drum, inverse spectral problems for elliptic operators and a partial resolution of the Weyl-Berry conjecture*, Trans. Amer. Math. Soc. **325**, no. 2, pp. 465–529 (1991).

[16] Lapidus, M. L., J. W. Neuberger, R. L. Renka, and C. A. Griffith, *Snowflake Harmonics and Computer Graphics: Numerical Computation of Spectra on Fractal Drums*, International Journal Bifurcation and Chaos **6**, no. 7, pp. 1185–1210 (1996).

[17] Lapidus, M. and M. Pang, *Eigenfunctions of the Koch snowflake domain*, Comm. Math. Phys. **172**, no. 2, pp. 359–376 (1995).

[18] Lauterbach, R. and S. Maier, *Symmetry-breaking at non-positive solutions of semilinear elliptic equations*, Arch. Rational Mech. Anal. **126**, no. 4, pp. 299–331 (1994).

[19] Lehoucq, R. B., D. C. Sorensen, and C. Yang *ARPACK users' guide: Solution of large-scale eigenvalue problems with implicitly restarted Arnoldi methods. Software, Environments, and Tools.* Society for Industrial and Applied Mathematics (SIAM), Philadelphia, PA, 1998. xvi+142 pp.

[20] Li, Y. and Zhou, J. *Convergence Results of a Local Minimax Method for Finding Multiple Critical Points*, SIAM J. Sci. Comput. **24**, no. 3, pp. 865–885 (electronic), (2002).

[21] Matthews, P. C., *Automated Symmetry-Breaking Calculations*, LMS J. Computational Math. **7**, pp. 101–119, (2004).

[22] Neuberger, J. W., *Sobolev Gradients and Differential Equations*, Lecture Notes in Mathematics, **1670**. Springer-Verlag, Berlin, 1997. viii+150 pp.

[23] Neuberger, J. M., *A Numerical Method for Finding Sign-Changing Solutions of Superlinear Dirichlet Problems*, Nonlinear World **4**, no. 1, pp. 73–83, (1997).

[24] Neuberger, J. M., *GNGA: Recent Progress and Open Problems for Semilinear Elliptic PDE*, Variational methods: open problems, recent progress, and numerical algorithms, Contemp. Math., **357**, Amer. Math. Soc., Providence, RI, pp. 201–237, (2004).

[25] Neuberger, J. M., *Nonlinear Elliptic Partial Difference Equations on Graphs*, J. Experimental Math, **15**, no. 1, pp. 91–107, (2005).

[26] Neuberger, J. M. and J. W. Swift *Newton's Method and Morse Index for Semilinear Elliptic PDEs* Internat. J. Bifur. Chaos Appl. Sci. Engrg. **11**, no. 3, pp. 801–820, (2001).

[27] Neuberger, J. M., N. Sieben and J. W. Swift, *Computing Eigenfunctions on the Koch Snowflake: A New Grid and Symmetry*, J. Comput. Appl. Math. **191**, no. 1, pp. 126–142, (2005).

[28] Rabinowitz, P., *Minimax Methods in Critical Point Theory with Applications to Differential Equations*, CBMS Regional Conference Series in Mathematics, **65**. Published for the Conference Board of the Mathematical Sciences, Washington, DC; by the American Mathematical Society, Providence, RI, 1986. viii+100 pp.
[29] Scott, W. R., *Group theory*, Prentice-Hall, Inc., Englewood Cliffs, N.J. 1964. xi+479 pp.
[30] Smoller, J. and A. G. Wasserman, *Symmetry-Breaking for Positive Solutions of Semilinear Elliptic Equations*, Archives of Rational Mechanics Analysis **95**, pp. 217–225 (1986).
[31] Sternberg, S., *Group Theory and Physics*, Cambridge University Press, Cambridge, 1994. xiv+429 pp.
[32] Thomas, A. D. and G. V. Wood, *Group Tables*, Shiva Mathematics Series, **2**. Shiva Publishing Ltd., Nantwich; distributed by Birkhser Boston, Inc., Cambridge, Mass., 1980. 174 pp.
[33] Thompson, T. J., *Estimating Solutions for the Ginzburg-Landau Superconductivity Model in Thin Disks*, M. S. Thesis, Northern Arizona University, (2005).
[34] Tinkham, M., *Group Theory and Quantum Mechanics*, McGraw-Hill Book Co., New York-Toronto, Ont.-London, 1964. xii+340 pp.
[35] Wang, Z-Q and J. Zhou, *A Local Minimax-Newton Method for Finding Multiple Saddle Points with Symmetries*, SIAM J. Numer. Anal. **42**, no. 4, pp. 1745–1759 (electronic), (2004).
[36] Wang, Z-Q and J. Zhou, *An Efficient and Stable Method for Computing Saddle Points with Symmetries*, SIAM J. Numer. Anal., **43**, no 2, pp. 891–907 (electronic), (2005).

*E-mail address*: John.Neuberger@nau.edu, Nandor.Sieben@nau.edu, Jim.Swift@nau.edu

Department of Mathematics and Statistics, Northern Arizona University PO Box 5717, Flagstaff, AZ 86011-5717, USA